IEEE Access
Multidisciplinary | Rapid Review | Open Access Journal

Received February 15, 2020, accepted February 26, 2020, date of publication March 9, 2020, date of current version March 19, 2020.

Digital Object Identifier 10.1109/ACCESS.2020.2979193

Robust Trajectory and Power Control for Cognitive UAV Secrecy Communication

YING GAO[1,2], HONGYING TANG[1], BAOQING LI[1], AND XIAOBING YUAN[1]

[1]Science and Technology on Microsystem Laboratory, Shanghai Institute of Microsystem and Information Technology, Chinese Academy of Sciences, Shanghai 201800, China

[2]University of Chinese Academy of Sciences, Beijing 100049, China

Corresponding author: Baoqing Li (sinoiot@mail.sim.ac.cn)

This work was supported in part by the National Natural Science Foundation of China under Grant 61901457, and in part by the Research Fund of Science and Technology on Microsystem Laboratory under Grant 6142804010304.

ABSTRACT This paper investigates the physical layer security issue in an unmanned aerial vehicle (UAV) aided cognitive radio network. Specially, a UAV operates as an aerial secondary transmitter to serve a ground secondary receiver (SR) by sharing the licensed wireless spectrum assigned to primary terrestrial communication networks, and in the meantime multiple eavesdroppers (Eves) try to wiretap the legitimate UAV-to-SR link. Under the assumption that the location formation of the Eves is imperfect, we jointly optimize the robust trajectory and transmit power of the UAV over a finite flight period to maximize the SR's average worst-case secrecy rate, while controlling the co-channel interference imposed on the primary receivers (PRs) below a tolerable level. The design is formulated as a non-convex semi-infinite optimization problem that is challenging to be optimally solved. To deal with it, we first prove that the considered problem can be simplified as a more tractable one, which resolves the location uncertainties of the Eves without the aid of $\mathcal{S}$-Procedure adopted in conventional methods. After that, an efficient iterative algorithm based on successive convex approximation (SCA) is developed to obtain a locally optimal solution. Numerical simulations are provided to demonstrate the effectiveness of our proposed algorithm and offer important system design insights.

INDEX TERMS UAV communications, cognitive radio, physical layer security, trajectory optimization, robust design.

I. INTRODUCTION

For the past few years, unmanned aerial vehicles (UAVs) have found widespread promising applications in the field of wireless communications due to their several advantages, such as highly controllable mobility, the ability of on-demand deployment, and line-of-sight (LoS) air-to-ground links [1]. For example, UAVs can be employed as aerial base stations (BSs) [2] to provide wireless service for a set of ground users, mobile relays [3] to deliver the source data to a remote destination node, or mobile data collectors [4] for wireless sensor networks.

Previous researches on UAV-enabled wireless communications can be loosely divided into two types. One type considers the application of UAVs as quasi-static BSs. Specifically, the UAVs' horizontal positions, altitudes and/or spatial density can be optimized to maximize the communication coverage area [5], [6], minimize the number of required UAV BSs [7], or maximize the number of covered users [8]–[10]. To fully exploit the high mobility of UAVs, the other type considers the application scenarios where UAVs are employed as mobile BSs/relays/access points/energy transmitters, whose locations over time (i.e., trajectories) can be properly designed to improve the communication performance. For example, a trajectory optimization problem is studied in [11] for completion time minimization in UAV-enabled multicasting. The authors in [12] investigate the jointly optimal 3D UAV trajectory and resource allocation algorithm design for a multicarrier solar-powered UAV communication system, with the goal of maximizing the system sum throughput. For a rotary-wing UAV-enabled wireless communication system, the work [13] studies the joint optimization of UAV trajectory, communication scheduling and mission completion time to minimize the UAV energy

The associate editor coordinating the review of this manuscript and approving it for publication was Xiaofei Wang.

consumption. In addition, UAV trajectory optimization or path planning has been widely investigated in various other applications such as multi-UAV communications [14], UAV-enabled wireless power transfer [15], mobile-edge computing [16], [17], and UAV-enabled data harvesting [18].

Despite the appealing benefits brought by UAVs, the broadcast nature of LoS channels brings a severe challenge to the information security of UAV-ground communications, since confidential messages are more vulnerable to be eavesdropped by unauthorized ground nodes. As an alternative to conventional cryptographic methods, physical layer security has become an appealing solution to cope with the security threats in UAV networks by exploiting the physical characteristics of wireless channels [19]. In general, the secrecy rate is considered as the key design metric to measure the physical layer security performance, which stands for the rate of confidential information can be reliably conveyed without being divulged to any eavesdroppers [20].

Recently, UAV-enabled secure communications have been extensively studied in the literature. As summarized by [21], emerging physical layer security strategies against eavesdropping in UAV wireless communication systems include trajectory optimization, resource allocation, robust design, artificial noise, and cooperation among multiple UAVs. Specifically, to maximize the secrecy rate, joint trajectory and transmit power design schemes are presented in [22] for a single-UAV communication system with a ground node and a potential eavesdropper. A joint user scheduling, UAV trajectory and transmit power control optimization framework is proposed in [23] for a downlink transmission scenario, where a UAV serves multiple users in a time division multiple access (TDMA) manner in the presence of an eavesdropper. The authors in [24]–[26] investigate the physical layer security for UAV-enabled mobile relaying systems. Reference [24] optimizes the UAV trajectory together with the transmit power of the source/UAV to secure the data transmission. In [25], caching is leveraged to improve the secrecy rate of the system. A secrecy energy efficiency (SEE) maximization problem is studied in [26], where SEE is defined as the ratio of the secrecy rate to the UAV energy consumption measured by bits-per-Joule (bits/J). In [27], a joint power control and trajectory optimization problem is investigated for UAV-enabled secure communications with no-fly zone constraints. Besides being employed as a transmitter or mobile relay, the UAV can also work as a friendly jammer that sends jamming signals to combat against eavesdropping attack. For example, [28] considers a scenario where a UAV jammer helps secure ground wiretap channels. Furthermore, a two-UAV scenario has been studied in several prior works, where one UAV transmits the confidential messages to the legitimate users, and the other cooperative UAV jams the eavesdroppers (e.g., [29]–[31]). The authors in [32] consider a cooperative secure communication system with multiple source UAVs and jamming UAVs. The SEE of the system is maximized by jointly optimizing the UAVs' trajectories, transmit power and user scheduling.

In addition, some prior works also take into account the imperfect location information of eavesdroppers (e.g., [33]–[37]), which is more suitable for practical applications. A joint robust trajectory and transmit power design framework is proposed in [33] for a single-UAV wireless network with a legitimate receiver and multiple eavesdroppers each located in an uncertain region. Compared with [33], an extra UAV is employed as a cooperative jammer in [34] to confuse an eavesdropper. In [35], the authors consider a scenario where a UAV acts as a friendly jammer to help secure communications between a legitimate on-ground transmitter-receiver pair for unknown eavesdropper location. For a UAV-enabled orthogonal frequency division multiple access (OFDMA) communication system, the authors in [36] jointly optimize the user scheduling, power allocation, UAV's trajectory and flight velocity to maximize the system energy efficiency. In [37], the authors investigate energy-efficient computation offloading problems in the presence of an active and a passive eavesdropper, respectively, for a secure UAV-edge-computing system.

Note that all the aforementioned works have assumed that the UAV communications are operated over dedicated frequency bands. Nevertheless, the problem of spectrum scarcity becomes increasingly severe due to the dramatic growth of mobile terminals, which makes it practically hard to assign dedicated spectrum to new UAV communications. In this regard, cognitive radio (CR) technology has been widely accepted as a promising approach to heighten the spectrum utilization ratio and ease the condition of spectrum scarcity [38]. Therefore, using UAVs in CR network can combine the benefits of both. A novel cognitive UAV communication paradigm is proposed in [39], where a UAV is employed as a cognitive/secondary transmitter to communicate with a secondary receiver (SR) in the presence of a set of primary terrestrial communication links that operate over the same frequency band. The authors jointly optimize the UAV trajectories and transmit power to maximize the SR's achievable rates under the quasi-stationary and mobile UAV scenarios, respectively, while ensuring that the interference power at the primary receivers (PRs) must be less than a given threshold. However, the work in [39] does not take the issue of UAV network security into account. Currently, only limited research efforts have been devoted to the physical layer security enhancement for UAV-aided CR networks. In [40], the authors deploy a UAV as a secondary relay to bridge the communication between a secondary transmitter-receiver pair in the presence of a PR that operate over the same frequency band and a potential eavesdropper. Reference [41] considers a scenario where a UAV is introduced as a friendly jammer to help improve the secrecy rate performance of a CR network. However, only one eavesdropper with perfect location information and one PR are considered in [40] and [41], which is overly optimistic and extremely simplifies the practical consideration.

Motivated by the above observations, we investigate in this paper a UAV-aided secure CR network, where a secondary

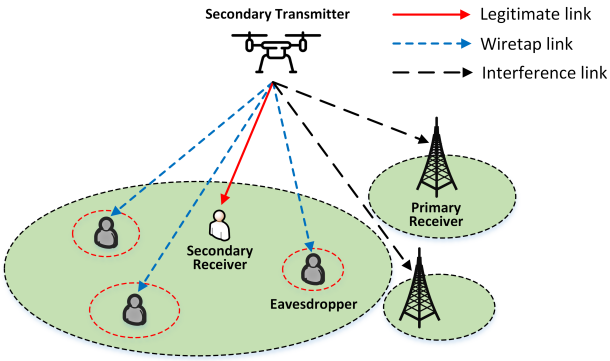

FIGURE 1. Illustration of a cognitive UAV secrecy communication system.

UAV transmitter sends confidential information to a ground SR in the presence of multiple PRs that operate over the same frequency band and multiple eavesdroppers (Eves), as shown in Fig. 1. It is assumed that the Eves' locations are only partially known to the UAV, subject to norm-bounded errors. For protecting the primary communications, we adopt the *interference temperature* (IT) technique in CR networks [42]. Accordingly, the interference imposed from the UAV transmit power to each PR must be below a given IT threshold. Our target is to maximize the SR's average worst-case secrecy rate through jointly designing the UAV's transmit power and trajectory over a finite flight duration with predetermined initial and final locations, subject to the mobility and transmit power constraints of the UAV, and the IT constraints at the PRs. The consequent problem is a non-convex semi-infinite optimization problem that is hard to solve optimally. Note that the trajectory optimization methods proposed in [39] for cognitive UAV communications do not take into account the security issue, thus can not be directly applied to our considered problem. Besides, in comparison with the prior studies on cognitive UAV secrecy communications (i.e., [40] and [41]), we consider multiple Eves with imperfect location information and multiple PRs, which in return brings challenge in robust trajectory and power design. In this paper, we develop an efficient suboptimal iterative algorithm for the considered problem by exploiting the properties of it and the advantages of successive convex approximation (SCA).

For clarity, the main contributions of this work are summarized as follows.

- We consider an average worst-case secrecy rate maximization problem in a UAV-aided secure CR network with multiple Eves each located in an uncertain region. To our best knowledge, this is a novel optimization problem and has not yet been studied in the literature.
- To tackle the formulated non-convex semi-infinite optimization problem, we first provide some useful insights to simplify it into a more tractable one, which resolves the location uncertainties of the Eves without the aid of $\mathcal{S}$-Procedure [43] adopted in conventional methods (e.g. in [33]). Then, an efficient iterative algorithm is proposed to obtain a locally optimal solution by leveraging the SCA technique.
- Numerical results demonstrate that the proposed joint design algorithm can enhance the secrecy rate performance in comparison with other benchmark schemes without trajectory optimization and/or power control. Besides, some important insights are provided in the simulations for the impact of IT threshold on the system performance.

The rest of this paper is organized as follows. Section II introduces the system model and the problem formulation for a cognitive UAV secrecy communication system. In Section III, we propose an efficient suboptimal algorithm for the considered problem. Simulation results are given in Section IV to demonstrate the efficacy of the proposed design, followed by conclusions in Section V.

Notations: In this paper, scalars and column vectors are written in italic and boldface lower-case letters, respectively. $\mathbb{R}^{M\times 1}$ denotes the space of M-dimensional real-valued vector. For a scalar x, its absolute value is denoted by $|x|$. For a vector $\boldsymbol{a}$, $\boldsymbol{a}^T$ represents its transpose and $\|\boldsymbol{a}\|$ denotes its Euclidean norm. For two points A and B in a three-dimensional Cartesian coordinate, $|AB|$ denotes the Euclidean distance between the two points. For two sets $\mathcal{K}_1$ and $\mathcal{K}_2$, $\mathcal{K}_1 \subseteq \mathcal{K}_2$ represents that $\mathcal{K}_1$ is a subset of $\mathcal{K}_2$.

II. SYSTEM MODEL AND PROBLEM FORMULATION

A. SYSTEM MODEL

As shown in Fig. 1, we consider the secrecy transmission in a UAV-aided CR network, which is composed of one secondary UAV transmitter, one SR, K Eves and L PRs. All the devices are assumed to be equipped with a single antenna. Without loss of generality, we express locations in a three-dimensional Cartesian coordinate system with all dimensions measured in meters (m). Suppose that the SR locates at $(x_s, y_s, 0)$, and the location of each Eve $k \in \mathcal{K} \triangleq \{1, \cdots, K\}$ is $(x_{e,k}, y_{e,k}, 0)$, where $\boldsymbol{w}_s = [x_s, y_s]^T \in \mathbb{R}^{2\times 1}$ and $\boldsymbol{w}_{e,k} = [x_{e,k}, y_{e,k}]^T \in \mathbb{R}^{2\times 1}$ denote the horizontal locations of the SR and Eve k, respectively. It is assumed that the UAV knows the exact location of the SR via proper information exchange, but only has the estimated horizontal location of Eve k, denoted by $\tilde{\boldsymbol{w}}_{e,k} = [\tilde{x}_{e,k}, \tilde{y}_{e,k}]^T \in \mathbb{R}^{2\times 1}$, with the estimation error being $\Delta\boldsymbol{w}_{e,k} = \boldsymbol{w}_{e,k} - \tilde{\boldsymbol{w}}_{e,k} = [\Delta x_{e,k}, \Delta y_{e,k}]^T \in \mathbb{R}^{2\times 1}$.[1] The estimation error satisfies

$$\Delta x_{e,k}^2 + \Delta y_{e,k}^2 \le \varepsilon_k^2, \tag{1}$$

from which we have

$$\boldsymbol{w}_{e,k} \in \mathcal{A}_{e,k} \triangleq \left\{ \boldsymbol{w}_{e,k} \middle| \left\| \boldsymbol{w}_{e,k} - \tilde{\boldsymbol{w}}_{e,k} \right\|^2 \le \varepsilon_k^2 \right\}, \tag{2}$$

[1] We assume that the SR can obtain its location via the global position systems (GPS) and/or other location techniques and then reports the location information to the UAV. However, owing to the lack of cooperation between the UAV and Eve k, the UAV can only obtain Eve k's estimated location by an camera or synthetic aperture radar. Such location estimation is expected suffering from errors since Eve k may keep silent to hide its existence [33].

where $\mathcal{A}_{e,k}$ represents the set of Eve k's possible locations. Accordingly, Eve k can be seen as locating in an uncertain circular region with a radius of ε_k centered at $(\tilde{x}_{e,k}, \tilde{y}_{e,k}, 0)$. For $l \in \mathcal{L} \triangleq \{1, \cdots, L\}$, PR l is assumed to locate at $(x_{p,l}, y_{p,l}, H_l)$ with $\boldsymbol{w}_{p,l} = [x_{p,l}, y_{p,l}]^T \in \mathbb{R}^{2\times 1}$ denoting its horizontal location and H_l representing its altitude.[2]

We assume that the UAV flies from the pre-determined initial location (x_I, y_I, H) to the final location (x_F, y_F, H) within the flight period T. Define $\boldsymbol{q}_I = [x_I, y_I]^T \in \mathbb{R}^{2\times 1}$ and $\boldsymbol{q}_F = [x_F, y_F]^T \in \mathbb{R}^{2\times 1}$ as the horizontal initial and final locations. For avoiding unnecessary energy consumption on frequent ascending or descending, the UAV is assumed to fly at a constant altitude H, the value of which corresponds to the minimum altitude required for terrain or building avoidance [44]. For ease of design, the flight period T is equally discretized into N time slot with step size $\delta = T/N$, which is set sufficiently small such that the change in the UAV's location within each time slot can be neglected [14]. As such, we can characterize the UAV trajectory projected on the horizontal plane as $\boldsymbol{q}[n] = [x[n], y[n]]^T \in \mathbb{R}^{2\times 1}$, $n \in \mathcal{N} \triangleq \{1, \cdots, N\}$. Let $D = V_{\max}\delta$ denote the maximum flying distance of the UAV within one time slot, where $V_{\max}$ is the maximum speed in meter/second (m/s). In practice, the UAV trajectory is limited by the following mobility constraints:

$$\|\boldsymbol{q}[n+1] - \boldsymbol{q}[n]\| \le D, n \in \mathcal{N} \setminus \{N\}, \tag{3a}$$

$$\|\boldsymbol{q}[1] - \boldsymbol{q}_I\| \le D, \ \boldsymbol{q}[N] = \boldsymbol{q}_F. \tag{3b}$$

Furthermore, in any time slot n, the distances from the UAV to the SR, Eve k and PR l can be expressed as $d_s[n] = \sqrt{\|\boldsymbol{q}[n] - \boldsymbol{w}_s\|^2 + H^2}$, $d_{e,k}[n] = \sqrt{\|\boldsymbol{q}[n] - \boldsymbol{w}_{e,k}\|^2 + H^2}$ and $d_{p,l}[n] = \sqrt{\|\boldsymbol{q}[n] - \boldsymbol{w}_{p,l}\|^2 + (H - H_l)^2}$, respectively.

It has been verified by the measurement results in [45]–[47] that the practical air-to-ground communication channels are mainly dominated by the LoS links, especially when the UAV flies in certain environment like rural or sub-urban areas with little blockage and scattering, and/or operates beyond a certain altitude. Additionally, the LoS-dominating air-to-ground channel model is also one of the considered channel models in the recent 3GPP specification [48]. As a result, to illustrate the most essential design insights and for ease of exposition in this paper, we adopt the widely-used LoS channel model for the UAV-to-ground links as in the prior works [22]–[34], [36], [37], [39]–[41]. The extension to the probabilistic LoS and Rician fading channels will be left as our future work. Besides, the Doppler effect brought by the UAV mobility is assumed to be perfectly compensated at the receivers based on existing techniques [49]. As a result, the channel power gain from the UAV to the SR in time slot n can be expressed as

$$h_s[n] = \beta_0 d_s^{-\alpha}[n] = \frac{\beta_0}{\left(\|\boldsymbol{q}[n] - \boldsymbol{w}_s\|^2 + H^2\right)^{\alpha/2}}, \tag{4}$$

[2]It is seen from Fig. 1 that the PRs in our considered scenario are ground BSs, whose locations are fixed and can be easily obtained by the UAV in advance.

where β_0 denotes the channel power gain from the UAV to the SR at the unit reference distance, and $\alpha \ge 2$ represents the generic path loss exponent determined by the radio propagation environment. Similarly, the channel power gains from the UAV to Eve k and PR l in time slot n are respectively given by

$$h_{e,k}[n] = \beta_0 d_{e,k}^{-\alpha}[n] = \frac{\beta_0}{\left(\|\boldsymbol{q}[n] - \boldsymbol{w}_{e,k}\|^2 + H^2\right)^{\alpha/2}}, \tag{5}$$

$$h_{p,l}[n] = \beta_0 d_{p,l}^{-\alpha}[n] = \frac{\beta_0}{\left(\|\boldsymbol{q}[n] - \boldsymbol{w}_{p,l}\|^2 + (H - H_l)^2\right)^{\alpha/2}}. \tag{6}$$

Denote the transmit power of the UAV in time slot n by $p[n]$, which needs to satisfy

$$0 \le p[n] \le P_{\max}, \quad \forall n, \tag{7a}$$

$$\frac{1}{N}\sum_{n=1}^{N} p[n] \le \bar{P}, \tag{7b}$$

where $P_{\max}$ and $\bar{P}$ denote the maximum peak power and average power given *a priori*, respectively. Note that (7b) corresponds to the total communication related power budget. Besides, to guarantee that (7b) is a non-trivial constraint, we assume that $\bar{P} < P_{\max}$. Then, we can express the achievable rate from the UAV to the SR in time slot n in bits/second/Hertz (bps/Hz) as

$$R_s[n] = \log_2\left(1 + \frac{h_s[n]p[n]}{\sigma^2}\right) = \log_2\left(1 + \frac{\gamma_0 p[n]}{\left(\|\boldsymbol{q}[n] - \boldsymbol{w}_s\|^2 + H^2\right)^{\alpha/2}}\right), \tag{8}$$

where $\gamma_0 \triangleq \beta_0/\sigma^2$ with σ^2 denoting the noise power at the receiver. Similarly, the achievable rate from the UAV to Eve k in time slot n in bps/Hz is given by

$$R_{e,k}[n] = \log_2\left(1 + \frac{\gamma_0 p[n]}{\left(\|\boldsymbol{q}[n] - \boldsymbol{w}_{e,k}\|^2 + H^2\right)^{\alpha/2}}\right). \tag{9}$$

Since the location information of each Eve is imperfect, the maximal achievable rate of Eve k in time slot n can be expressed as $\max_{\boldsymbol{w}_{e,k}\in\mathcal{A}_{e,k}} R_{e,k}[n]$. Accordingly, the worst-case secrecy rate of the SR, in the presence of K Eves, in time slot n in bps/Hz can be written as

$$R_{\text{sec}}[n] = \left[R_s[n] - \max_{k\in\mathcal{K}} \max_{\boldsymbol{w}_{e,k}\in\mathcal{A}_{e,k}} R_{e,k}[n]\right]^+, \tag{10}$$

where $[x]^+ \triangleq \max(x, 0)$, which makes function (10) non-smooth at zero value.

In such a spectrum sharing scenario, the terrestrial PRs suffer from the air-to-ground co-channel interference introduced by the secondary UAV communication. In a certain time slot n, the interference power at PR l is given by

$$Q[n] = h_{p,l}[n]p[n] = \frac{\beta_0 p[n]}{\left(\|\boldsymbol{q}[n] - \boldsymbol{w}_{p,l}\|^2 + (H - H_l)^2\right)^{\alpha/2}}. \tag{11}$$

To protect the primary communications, we apply the widely adopted IT technique as in [39], [42]. Accordingly, in each time slot n, the UAV's interference power at PR l should be limited below a threshold, denoted by $\Gamma_l \geq 0$. We thus have

$$\frac{\beta_0 p[n]}{\left(\|\boldsymbol{q}[n]-\boldsymbol{w}_{p,l}\|^2+(H-H_l)^2\right)^{\alpha/2}} \leq \Gamma_l. \tag{12}$$

B. PROBLEM FORMULATION

Our objective is to maximize the SR's average worst-case secrecy rate over the total N time slots (i.e., $\frac{1}{N}\sum_{n=1}^{N} R_{\text{sec}}[n]$), by jointly optimizing the UAV's trajectory $\{\boldsymbol{q}[n], \forall n\}$ and transmit power $\{p[n], \forall n\}$, constrained by the UAV mobility constraints in (3), the transmit power constraints in (7) and the IT constraints in (12). Mathematically, the investigated problem can be formulated as

$$\begin{aligned}
(\text{P1}): \max_{\{\boldsymbol{q}[n],p[n]\}} \ & \frac{1}{N}\sum_{n=1}^{N}\left[R_s[n]-\max_{k\in\mathcal{K}}\max_{\boldsymbol{w}_{e,k}\in\mathcal{A}_{e,k}} R_{e,k}[n]\right] && \text{(13a)}\\
\text{s.t. } & \|\boldsymbol{q}[n+1]-\boldsymbol{q}[n]\| \leq D, n\in\mathcal{N}\setminus\{N\}, && \text{(13b)}\\
& \|\boldsymbol{q}[1]-\boldsymbol{q}_I\| \leq D,\ \boldsymbol{q}[N]=\boldsymbol{q}_F, && \text{(13c)}\\
& 0\leq p[n]\leq P_{\max},\ \forall n, && \text{(13d)}\\
& \frac{1}{N}\sum_{n=1}^{N} p[n]\leq \bar{P}, && \text{(13e)}\\
& \frac{\beta_0 p[n]}{\left(\|\boldsymbol{q}[n]-\boldsymbol{w}_{p,l}\|^2+(H-H_l)^2\right)^{\alpha/2}} \leq \Gamma_l,\ \forall n,l, && \text{(13f)}
\end{aligned}$$

where the operation $[\cdot]^+$ has been dropped in (13a), since for any time slot n, the corresponding summation term in the objective function, i.e., $R_s[n]-\max_{k\in\mathcal{K}}\max_{\boldsymbol{w}_{e,k}\in\mathcal{A}_{e,k}} R_{e,k}[n]$, must be non-negative at the optimal solution; otherwise, its value can be increased to zero by setting $p[n]=0$ without violating the power-related constraints (13d)-(13f). As such, problem (P1) resolves the non-smooth issue brought by the operation $[\cdot]^+$.

Remark 1: It is not hard to see that the minimum required time length for the UAV to fly from the pre-determined initial location to the final location is given by $T_{\min} = \|\boldsymbol{q}_F-\boldsymbol{q}_I\|/V_{\max}$. Obviously, there must be $T \geq T_{\min}$ to ensure the feasibility of trajectory design. Note that when $T \geq T_{\min}$, we can alway find feasible solutions to problem (P1) that meet all the constraints. Therefore, the feasibility condition of (P1) is just $T \geq T_{\min}$.

Problem (P1) is challenging to solve for the following three aspects. First, due to the uncertainty in each Eve's location, (P1) is an intractable semi-infinite optimization problem. Second, the objective function is non-concave due to the coupling of optimization variables $\boldsymbol{q}[n]$ and $p[n]$. Third, (13f) is not jointly convex with respect to $\boldsymbol{q}[n]$ and $p[n]$. In general, there is no standard method to solve such a non-convex problem optimally. In Section III, we will propose an efficient algorithm to find a locally optimal solution for (P1).

III. PROPOSED ALGORITHM FOR PROBLEM (P1)

In this section, we develop an efficient algorithm to solve problem (P1) sub-optimally. Specially, we first provide some useful insights to simplify problem (P1) into a more tractable one, which resolves the location uncertainties of the Eves. After that, for the resulting non-convex optimization problem, we propose an efficient iterative algorithm to obtain a locally optimal solution with the assistance of the SCA technique. In the end, we summarize the overall algorithm and propose an efficient initialization scheme for it.

A. SIMPLIFICATION OF PROBLEM (P1)

For problem (P1), since each Eve's uncertain location parameter $\boldsymbol{w}_{e,k}$ only exists in the expression for $R_{e,k}[n]$, we first derive an explicit expression for $\max_{\boldsymbol{w}_{e,k}\in\mathcal{A}_{e,k}} R_{e,k}[n]$. Notice that by referring to (9), we have

$$\begin{aligned}
&\max_{\boldsymbol{w}_{e,k}\in\mathcal{A}_{e,k}} R_{e,k}[n]\\
&= \log_2\left(1+\frac{\gamma_0\, p\,[n]}{\left(\min\limits_{\boldsymbol{w}_{e,k}\in\mathcal{A}_{e,k}}\|\boldsymbol{q}\,[n]-\boldsymbol{w}_{e,k}\|^2+H^2\right)^{\alpha/2}}\right),
\end{aligned} \tag{14}$$

where we have used the fact that the expression for $R_{e,k}[n]$ is monotonically decreasing with respect to $\|\boldsymbol{q}[n]-\boldsymbol{w}_{e,k}\|^2$. This thus motivates us to consider the following problem:

$$\min_{\boldsymbol{w}_{e,k}\in\mathcal{A}_{e,k}} \|\boldsymbol{q}[n]-\boldsymbol{w}_{e,k}\|^2. \tag{15}$$

It is not difficult to verify that the optimal value of (15) is attained at $\boldsymbol{w}^*_{e,k}(\boldsymbol{q}[n]) = \tilde{\boldsymbol{w}}_{e,k} + \frac{\boldsymbol{q}[n]-\tilde{\boldsymbol{w}}_{e,k}}{\|\boldsymbol{q}[n]-\tilde{\boldsymbol{w}}_{e,k}\|}\varepsilon_k$ when $\|\boldsymbol{q}\,[n]-\tilde{\boldsymbol{w}}_{e,k}\| \geq \varepsilon_k$, and $\boldsymbol{w}^*_{e,k}(\boldsymbol{q}[n]) = \mathbf{q}[n]$ otherwise. Accordingly, we have

$$\begin{aligned}
&\min_{\boldsymbol{w}_{e,k}\in\mathcal{A}_{e,k}} \|\boldsymbol{q}[n]-\boldsymbol{w}_{e,k}\|^2\\
&= \begin{cases} \left|\,\|\boldsymbol{q}\,[n]-\tilde{\boldsymbol{w}}_{e,k}\|-\varepsilon_k\right|^2, & \|\boldsymbol{q}\,[n]-\tilde{\boldsymbol{w}}_{e,k}\| \geq \varepsilon_k,\\ 0, & \|\boldsymbol{q}\,[n]-\tilde{\boldsymbol{w}}_{e,k}\| < \varepsilon_k. \end{cases}
\end{aligned} \tag{16}$$

By substituting the solution in (16) back into (14), we have

$$\begin{aligned}
&\max_{\boldsymbol{w}_{e,k}\in\mathcal{A}_{e,k}} R_{e,k}[n]\\
&= \begin{cases} \hat{R}_{e,k}[n], & \|\boldsymbol{q}\,[n]-\tilde{\boldsymbol{w}}_{e,k}\| \geq \varepsilon_k,\\ \log_2\left(1+\dfrac{\gamma_0 p[n]}{(H^2)^{\alpha/2}}\right), & \|\boldsymbol{q}\,[n]-\tilde{\boldsymbol{w}}_{e,k}\| < \varepsilon_k, \end{cases}\\
&\triangleq \tilde{R}_{e,k}[n],
\end{aligned} \tag{17}$$

where

$$\hat{R}_{e,k}[n] \triangleq \log_2\left(1+\frac{\gamma_0 p[n]}{\left(\left|\,\|\boldsymbol{q}\,[n]-\tilde{\boldsymbol{w}}_{e,k}\|-\varepsilon_k\right|^2+H^2\right)^{\alpha/2}}\right). \tag{18}$$

Without loss of optimality to problem (P1), we replace the term $\max_{\boldsymbol{w}_{e,k}\in\mathcal{A}_{e,k}} R_{e,k}[n]$ in (13a) with the solution in (17),

and then rewrite the objective function of (P1) as

$$\frac{1}{N}\sum_{n=1}^{N}\left[R_s[n]-\max_{k\in\mathcal{K}}\tilde{R}_{e,k}[n]\right]. \tag{19}$$

However, since $\tilde{R}_{e,k}[n]$ is a piecewise function of the optimization variable $\boldsymbol{q}[n]$, problem (P1) with objective function (19) is still intractable. To handle the intractability, we first present the following lemma:

Lemma 1: In any time slot n, if $\|\boldsymbol{q}[n]-\tilde{\boldsymbol{w}}_{e,k}\|<\varepsilon_k$ for some certain $k\in\mathcal{K}$, we have $\min_{k\in\mathcal{K}}\left|\|\boldsymbol{q}[n]-\tilde{\boldsymbol{w}}_{e,k}\|-\varepsilon_k\right| < \|\boldsymbol{q}[n]-\boldsymbol{w}_s\|$.

Proof: See Appendix A.

Then, we introduce the following proposition:

Proposition 1: Problem (P1) is equivalent[3] to the following problem

$$\begin{aligned}(\text{P2}):\quad &\max_{\{\boldsymbol{q}[n],p[n]\}}\ \frac{1}{N}\sum_{n=1}^{N}\left[R_s[n]-\max_{k\in\mathcal{K}}\hat{R}_{e,k}[n]\right] \\ &\text{s.t. (13b)}-\text{(13f)}.\end{aligned} \tag{20}$$

Notice that in (P2), the expression for $\hat{R}_{e,k}[n]$ is in a deterministic form and does not change with the relationship of size between $\|\boldsymbol{q}[n]-\tilde{\boldsymbol{w}}_{e,k}\|$ and ε_k.

Proof: First of all, by substituting the expression for $R_s[n]$ in (8) and the expression for $\hat{R}_{e,k}[n]$ in (18) into (20), we can re-express the objective function of (P2) as shown in (21) (at the bottom of this page).

Next, denote M_1^* and M_2^* as the optimal values of problem (P1) and (P2), respectively. Note that we have $M_1^*\le M_2^*$, since $\tilde{R}_{e,k}[n]\ge\hat{R}_{e,k}[n]$. We then denote $(\boldsymbol{q}^*,\boldsymbol{p}^*)$ as the optimal solution to problem (P2), where $\boldsymbol{q}^*\triangleq\{\boldsymbol{q}^*[n],\forall n\}$ and $\boldsymbol{p}^*\triangleq\{p^*[n],\forall n\}$, which is also a feasible solution to problem (P1) due to the fact that (P1) and (P2) have the same constraints. Denote $\tilde{M}$ as the objective value of problem (P1) attained at $(\boldsymbol{q}^*,\boldsymbol{p}^*)$. Obviously, $\tilde{M}\le M_1^*$. Then, we are going to show that $\tilde{M}=M_2^*$. To this end, for any specific time slot n_0, we consider the following two different cases.

[3]Here, the word "equivalent" means that the two problems have the same optimal value.

1) CASE 1: $\|\boldsymbol{q}^*[n_0]-\tilde{\boldsymbol{w}}_{e,k}\|\ge\varepsilon_k,\forall k\in\mathcal{K}$

Since $\tilde{R}_{e,k}(\boldsymbol{q}^*[n_0],p^*[n_0])=\hat{R}_{e,k}(\boldsymbol{q}^*[n_0],p^*[n_0])$ in this case, it is easy to obtain that

$$\begin{aligned}&R_s\left(\boldsymbol{q}^*[n_0],p^*[n_0]\right)-\max_{k\in\mathcal{K}}\tilde{R}_{e,k}\left(\boldsymbol{q}^*[n_0],p^*[n_0]\right)\\ &=R_s\left(\boldsymbol{q}^*[n_0],p^*[n_0]\right)-\max_{k\in\mathcal{K}}\hat{R}_{e,k}\left(\boldsymbol{q}^*[n_0],p^*[n_0]\right).\end{aligned} \tag{22}$$

2) CASE 2: $\|\boldsymbol{q}^*[n_0]-\tilde{\boldsymbol{w}}_{e,k}\|<\varepsilon_k$ FOR SOME CERTAIN $k\in\mathcal{K}$

According to Lemma 1, we have

$$\min_{k\in\mathcal{K}}\left|\|\boldsymbol{q}^*[n_0]-\tilde{\boldsymbol{w}}_{e,k}\|-\varepsilon_k\right|<\|\boldsymbol{q}^*[n_0]-\boldsymbol{w}_s\|. \tag{23}$$

By observing problem (P2) with objective function (21), it is easy to see that (23) must lead to $p^*[n_0]=0$ at the optimal solution to problem (P2), since otherwise the transmit power allocated to time slot n_0 can be assigned to any other time slot for further secrecy performance improvement. It then follows that

$$\begin{aligned}&R_s\left(\boldsymbol{q}^*[n_0],p^*[n_0]\right)-\max_{k\in\mathcal{K}}\tilde{R}_{e,k}\left(\boldsymbol{q}^*[n_0],p^*[n_0]\right)\\ &=R_s\left(\boldsymbol{q}^*[n_0],p^*[n_0]\right)-\max_{k\in\mathcal{K}}\hat{R}_{e,k}\left(\boldsymbol{q}^*[n_0],p^*[n_0]\right)\\ &=0.\end{aligned} \tag{24}$$

With (22) and (24), we have $\tilde{M}=M_2^*$ and thus $M_1^*\ge M_2^*$. Therefore, $M_1^*=M_2^*$, which thus completes the proof of Proposition 1.

Remark 2: By exploiting the special structure of the considered problem, Proposition 1 avoids dealing with the piecewise objective function (19), yielding the more tractable problem (P2). Note that we can also apply the $\mathcal{S}$-Procedure [43] to tackle the location uncertainties of the Eves as in the existing work [33]. Compared with [33], our work avoids the introduction of a great deal of slack variables and high-dimensional linear matrix inequality (LMI) constraints. Besides, Proposition 1 can be directly applied to simplify the problem studied in [33].

According to Proposition 1, we only need to focus on solving problem (P2), which, however, is still non-convex due to the non-concave objective function and non-convex constraint (13f). In the following subsection, we will adopt the SCA technique to solve (P2) sub-optimally.

B. SCA-BASED ALGORITHM FOR PROBLEM (P2)

By introducing two sets of slack variables $[\mu_s[1],\cdots,\mu_s[N]]^T$ and $[\mu_e[1],\cdots,\mu_e[N]]^T$, and operating a simple

$$\begin{aligned}&\frac{1}{N}\sum_{n=1}^{N}\left[\log_2\left(1+\frac{\gamma_0\,p[n]}{\left(\|\boldsymbol{q}[n]-\boldsymbol{w}_s\|^2+H^2\right)^{\alpha/2}}\right)-\max_{k\in\mathcal{K}}\log_2\left(1+\frac{\gamma_0 p[n]}{\left(\left|\|\boldsymbol{q}[n]-\tilde{\boldsymbol{w}}_{e,k}\|-\varepsilon_k\right|^2+H^2\right)^{\alpha/2}}\right)\right]\\ &=\frac{1}{N}\sum_{n=1}^{N}\left[\log_2\left(1+\frac{\gamma_0\,p[n]}{\left(\|\boldsymbol{q}[n]-\boldsymbol{w}_s\|^2+H^2\right)^{\alpha/2}}\right)-\log_2\left(1+\frac{\gamma_0 p[n]}{\left(\min_{k\in\mathcal{K}}\left|\|\boldsymbol{q}[n]-\tilde{\boldsymbol{w}}_{e,k}\|-\varepsilon_k\right|^2+H^2\right)^{\alpha/2}}\right)\right].\end{aligned} \tag{21}$$

mathematical manipulation on constraint (13f), we can transform problem (P2) into the following equivalent form:

$$(\text{P3}): \quad \max_{\mathcal{Z}} \frac{1}{N}\sum_{n=1}^{N}\bar{R}_{\text{sec}}[n] \tag{25a}$$

$$\text{s.t. } \mu_s[n] \geq \left(\|\boldsymbol{q}[n]-\boldsymbol{w}_s\|^2+H^2\right)^{\alpha/2}, \ \forall n, \tag{25b}$$

$$\mu_e[n] \leq \left(\left|\|\boldsymbol{q}[n]-\tilde{\boldsymbol{w}}_{e,k}\|-\varepsilon_k\right|^2+H^2\right)^{\alpha/2}, \forall n,k, \tag{25c}$$

$$p[n] \leq \frac{\Gamma_l}{\beta_0}\left(\|\boldsymbol{q}[n]-\boldsymbol{w}_{p,l}\|^2+(H-H_l)^2\right)^{\alpha/2}, \forall n,l, \tag{25d}$$

$$(13b)-(13e),$$

where $\mathcal{Z} \triangleq \{\boldsymbol{q}[n], p[n], \mu_s[n], \mu_e[n]\}_{n=1}^N$ is the set of optimization variables, and

$$\bar{R}_{\text{sec}}[n]=\log_2\left(1+\frac{\gamma_0 p[n]}{\mu_s[n]}\right)-\log_2\left(1+\frac{\gamma_0 p[n]}{\mu_e[n]}\right). \tag{26}$$

The proof of equivalence between problem (P3) and (P2) can be referred in Appendix B. Next, we focus on solving problem (P3). Note that the objective function is not jointly concave with respective to $\boldsymbol{q}[n]$ and $p[n]$. Besides, the right-hand-sides (RHSs) of the constraints (25b) and (25d) are all convex with respect to $\boldsymbol{q}[n]$ (the proof is given in Appendix C). Therefore, constraint (25b) is convex, while constraint (25d) is non-convex since the super-level set of a convex quadratic function is not convex in general [43]. However, it is hard to tell whether constraint (25c) is convex. To tackle this issue, we introduce a set of slack variables $[t[1],\cdots,t[N]]^T$, and then convert constraint (25c) to

$$\mu_e[n] \leq t[n]^{\alpha/2}, \ \forall n, \tag{27a}$$

$$\begin{aligned} t[n] &\leq \left|\|\boldsymbol{q}[n]-\tilde{\boldsymbol{w}}_{e,k}\|-\varepsilon_k\right|^2+H^2 \\ &= \|\boldsymbol{q}[n]-\tilde{\boldsymbol{w}}_{e,k}\|^2-2\varepsilon_k\|\boldsymbol{q}[n]-\tilde{\boldsymbol{w}}_{e,k}\|+\varepsilon_k^2+H^2, \\ &\quad \forall n,k. \end{aligned} \tag{27b}$$

With this manipulation, problem (P3) can be equivalently transformed into

$$\begin{aligned} (\text{P4}): \quad &\max_{\tilde{\mathcal{Z}}} \frac{1}{N}\sum_{n=1}^{N}\bar{R}_{\text{sec}}[n] \\ &\text{s.t. } (13b)-(13e),(25b),(25d),(27a),(27b), \end{aligned}$$

where $\tilde{\mathcal{Z}} \triangleq \{\boldsymbol{q}[n], p[n], \mu_s[n], \mu_e[n], t[n]\}_{n=1}^N$. The equivalence between problem (P4) and (P3) can be found in Appendix D. Note that constraints (27a) and (27b) are non-convex due to the convexity of the terms $t[n]^{\alpha/2}$ and $\|\boldsymbol{q}[n]-\tilde{\boldsymbol{w}}_{e,k}\|^2$. Therefore, (P4) is a non-convex optimization problem, where the non-convexity arises from the objective function, and constraints (25d), (27a) and (27b). To address this issue, we intend to leverage the SCA technique to convert the non-convex problem (P4) approximately into a convex one. By iteratively solving a series of approximate convex problems, we can obtain a locally optimal solution to the original non-convex problem (P4).

Specially, denote the given local point in the r-th iteration by $\tilde{\mathcal{Z}}^r \triangleq \{\boldsymbol{q}^r[n], p^r[n], \mu_s^r[n], \mu_e^r[n], t^r[n]\}_{n=1}^N$.[4] Then, we rewrite the summation term $\bar{R}_{\text{sec}}[n]$ in (26) as

$$\begin{aligned} \bar{R}_{\text{sec}}[n] &= \log_2\left(\mu_s[n]+\gamma_0 p[n]\right)-\log_2\left(\mu_s[n]\right) \\ &\quad -\log_2\left(\mu_e[n]+\gamma_0 p[n]\right)+\log_2\left(\mu_e[n]\right). \end{aligned} \tag{29}$$

Note that in (29), the term $-\log_2(\mu_s[n])$ is convex with respect to $\mu_s[n]$, and the term $-\log_2(\mu_e[n]+\gamma_0 p[n])$ is jointly convex with respect to $\mu_e[n]$ and $p[n]$. These thus make (29) a non-concave function. Recall that any convex function is globally lower-bounded by its first-order Taylor expansion at any point [43]. Therefore, with given local point $\tilde{\mathcal{Z}}^r$ at iteration $r \geq 1$, we can obtain the global underestimator for $\bar{R}_{\text{sec}}[n]$ as shown in (30).

$$\begin{aligned} \bar{R}_{\text{sec}}[n] &\geq \log_2\left(\mu_s[n]+\gamma_0 p[n]\right)-\log_2\left(\mu_s^r[n]\right) \\ &\quad -\frac{\mu_s[n]-\mu_s^r[n]}{\mu_s^r[n]\ln 2}-\log_2\left(\mu_e^r[n]+\gamma_0 p^r[n]\right) \\ &\quad -\frac{\mu_e[n]-\mu_e^r[n]}{\left(\mu_e^r[n]+\gamma_0 p^r[n]\right)\ln 2} \\ &\quad -\frac{\gamma_0\left(p[n]-p^r[n]\right)}{\left(\mu_e^r[n]+\gamma_0 p^r[n]\right)\ln 2}+\log_2\left(\mu_e[n]\right) \triangleq \bar{R}_{\text{sec}}^{\text{lb},r}[n]. \end{aligned} \tag{30}$$

$$\begin{aligned} &\left(\|\boldsymbol{q}[n]-\boldsymbol{w}_{p,l}\|^2+(H-H_l)^2\right)^{\alpha/2} \\ &\geq \left(\|\boldsymbol{q}^r[n]-\boldsymbol{w}_{p,l}\|^2+(H-H_l)^2\right)^{\alpha/2} \\ &\quad +\alpha\left[\left(\|\boldsymbol{q}^r[n]-\boldsymbol{w}_{p,l}\|^2+(H-H_l)^2\right)^{\frac{\alpha}{2}-1}\right] \\ &\quad \times\left[\left(\boldsymbol{q}^r[n]-\boldsymbol{w}_{p,l}\right)^T\left(\boldsymbol{q}[n]-\boldsymbol{q}^r[n]\right)\right] \triangleq \mathcal{P}_{p,l}^{\text{lb},r}\left(\boldsymbol{q}[n]\right), \ \forall n,l. \end{aligned} \tag{31}$$

To proceed, we consider the non-convex constraints (25d), (27a) and (27b). Since the RHSs of (25d) and (27a), and the term $\|\boldsymbol{q}[n]-\tilde{\boldsymbol{w}}_{e,k}\|^2$ in (27b) are convex with respect to $\boldsymbol{q}[n]$, $t[n]$ and $\boldsymbol{q}[n]$, respectively, we have the inequalities in (31), (32) and (33) by applying the first-order Taylor expansions at given local point $\tilde{\mathcal{Z}}^r$.

$$\begin{aligned} t[n]^{\alpha/2} &\geq t^r[n]+\frac{\alpha}{2}\left(t^r[n]\right)^{\frac{\alpha}{2}-1}\left(t[n]-t^r[n]\right) \\ &\triangleq \mathcal{T}^{\text{lb},r}\left(t[n]\right), \forall n. \end{aligned} \tag{32}$$

$$\begin{aligned} \|\boldsymbol{q}[n]-\tilde{\boldsymbol{w}}_{e,k}\|^2 &\geq \|\boldsymbol{q}^r[n]-\tilde{\boldsymbol{w}}_{e,k}\|^2+2\left(\boldsymbol{q}^r[n]-\tilde{\boldsymbol{w}}_{e,k}\right)^T \\ &\quad \times\left(\boldsymbol{q}[n]-\boldsymbol{q}^r[n]\right) \triangleq \mathcal{E}_{e,k}^{\text{lb},r}\left(\boldsymbol{q}[n]\right), \ \forall n,k. \end{aligned} \tag{33}$$

Then, with (31), (32) and (33), we can approximate the non-convex constraints (25d), (27a) and (27b) as the following convex ones:

$$p[n] \leq \frac{\Gamma_l}{\beta_0}\cdot\mathcal{P}_{p,l}^{\text{lb},r}\left(\boldsymbol{q}[n]\right), \quad \forall n,l, \tag{34}$$

$$\mu_e[n] \leq \mathcal{T}^{\text{lb},r}\left(t[n]\right), \quad \forall n, \tag{35}$$

[4] In Algorithm 1 proposed in Section III-C, we show that $\tilde{\mathcal{Z}}^r$ is in fact the solution obtained from the $(r-1)$-th iteration, and $\tilde{\mathcal{Z}}^0$ stands for the initial point.

Algorithm 1 Proposed Algorithm for Problem (P1)

1: Construct the initial point $\tilde{\mathcal{Z}}^0$. Let $r = 0$.
2: **repeat**
3: Solve problem (P5) for the given local point $\tilde{\mathcal{Z}}^r$ and denote the optimal solution as $\tilde{\mathcal{Z}}^* \triangleq \{\boldsymbol{q}^*[n], p^*[n], \mu_s^*[n], \mu_e^*[n], t^*[n]\}_{n=1}^N$.
4: Update $\tilde{\mathcal{Z}}^{r+1} = \tilde{\mathcal{Z}}^*$.
5: Update $r = r + 1$.
6: **until** The fractional increase of the objective value is below a given maximum tolerance ϵ.

$$t[n] \le \mathcal{E}_{e,k}^{\mathrm{lb},r}(\boldsymbol{q}[n]) - 2\varepsilon_k\|\boldsymbol{q}[n] - \tilde{\boldsymbol{w}}_{e,k}\| + \varepsilon_k^2 + H^2, \forall n, k. \tag{36}$$

By summarizing the above developments, we obtain the following approximate problem (P5) for (P4) at the given local point $\tilde{\mathcal{Z}}^r$ in the r-th iteration:

$$(\mathrm{P5}): \max_{\tilde{\mathcal{Z}}} \frac{1}{N}\sum_{n=1}^{N} \bar{R}_{\mathrm{sec}}^{\mathrm{lb},r}[n] \quad \text{s.t. (13b)} - \text{(13e)}, \text{(25b)}, \text{(34)} - \text{(36)}.$$

Since the objective function is convex, and the feasible region is also convex, problem (P5) is a convex optimization problem, which can be efficiently solved by standard convex optimization solvers, e.g., CVX [43].[5]

C. OVERALL ALGORITHM

Since (P1) is an intractable non-convex semi-infinite optimization problem, finding the global optimal solution is exceedingly difficult in general. Based on the simplification and approximations presented in previous two subsections, an efficient suboptimal algorithm for problem (P1) is concluded in Algorithm 1. As depicted by the steps 3-5, we show that the given local point $\tilde{\mathcal{Z}}^r$ is in fact the solution obtained from the $(r-1)$-th iteration. The setup of the initial point $\tilde{\mathcal{Z}}^0$ will be given in Section III-D. A brief convergence analysis is given as follows. Since the optimal value of (P4) is finite, and the objective value of (P4) with the solution obtained by solving problem (P5) is non-decreasing after each iteration, Algorithm 1 is guaranteed to converge at a locally optimal solution to problem (P4) (and thus problem (P1)).

Next, the computational complexity of the proposed algorithm is discussed. Note that in each iteration, the complexity of Algorithm 1 is dominated by solving problem (P5) via the interior-point method invoked by CVX. Specifically, problem (P5) contains $N-1$ second-order cone (SOC) constraints of dimension 4, 1 SOC constraint of dimension 2, 2 linear inequality constraints (1 linear equality constraint) of dimension 2, $2N$ linear inequality constraints of dimension 1, 1 linear inequality constraint of dimension N, N SOC constraints of dimension 3, LN linear inequality constraints of dimension 3, N linear inequality constraint of dimension 2, and KN SOC constraints of dimension 3. The total number of optimization variables is $6N$. Based on the complexity analysis in [50], the computational cost of solving problem (P5) is about $\mathcal{O}\left[N^{3.5}\left(K^{1.5}+L^{1.5}\right)\right]$. As a result, the total complexity of Algorithm 1 is on the order of $\mathcal{O}\left[IN^{3.5}\left(K^{1.5}+L^{1.5}\right)\right]$ with I denoting the number of iterations needed for convergence.

[5] As a side note, constraint (25b) can be expressed in a canonical form that accepted by CVX with the aid of the function *pow_abs* or the functions *norm* and *square_pos* when $\alpha = 2$, and together with the function *pow_pos* when $\alpha > 2$.

D. INITIALIZATION SCHEME

In this subsection, we give a low-complexity initialization scheme for Algorithm 1 in three steps. First of all, the initial UAV trajectory $\{\boldsymbol{q}^0[n]\}_{n=1}^N$ adopts the heuristic best-effort manner as designed in [22], i.e., the UAV flies straightly from the initial location to the position right above the SR at speed $V_{\max}$, then hovers there with the maximum duration, and finally flies straightly at speed $V_{\max}$ to reach the final location by the end of the last time slot. In the case that the UAV dose not have sufficient time to reach the position right above the SR, it will turn at a certain midway point and then fly straightly to the final location at speed $V_{\max}$. Secondly, the slack variables $\{\mu_s^0[n]\}_{n=1}^N$, $\{t^0[n]\}_{n=1}^N$ and $\{\mu_e^0[n]\}_{n=1}^N$ are respectively set as

$$\mu_s^0[n] = \left(\|\boldsymbol{q}^0[n] - \boldsymbol{w}_s\|^2 + H^2\right)^{\alpha/2}, \ \forall n, \tag{38a}$$

$$t^0[n] = \min_{k\in\mathcal{K}} |\,\|\boldsymbol{q}^0[n] - \tilde{\boldsymbol{w}}_{e,k}\| - \varepsilon_k|^2 + H^2, \ \forall n, \tag{38b}$$

$$\mu_e^0[n] = t^0[n]^{\alpha/2}, \ \forall n. \tag{38c}$$

Finally, with given $\{\boldsymbol{q}^0[n], \mu_s^0[n], \mu_e^0[n], t^0[n]\}_{n=1}^N$, problem (P4) can be written as

$$\max_{p[n]} \frac{1}{N}\sum_{n=1}^{N}\left[\log_2(1+a_n p[n]) - \log_2(1+b_n p[n])\right] \tag{39a}$$

$$\text{s.t. } 0 \le p[n] \le P_{\max}, \ \forall n, \tag{39b}$$

$$\frac{1}{N}\sum_{n=1}^{N} p[n] \le \bar{P}, \tag{39c}$$

$$p[n] \le \frac{\Gamma_l}{\beta_0}\left(\|\boldsymbol{q}^0[n] - \boldsymbol{w}_{p,l}\|^2 + (H-H_l)^2\right)^{\alpha/2}, \ \forall n, l, \tag{39d}$$

where $a_n \triangleq \gamma_0/\mu_s^0[n]$ and $b_n \triangleq \gamma_0/\mu_e^0[n]$. We then simply set $p^0[n] = \min\left[\bar{P}, \min_{l\in\mathcal{L}} \frac{\Gamma_l}{\beta_0}\left(\|\boldsymbol{q}^0[n] - \boldsymbol{w}_{p,l}\|^2 + (H-H_l)^2\right)^{\alpha/2}\right]$ if $a_n \ge b_n$, and $p^0[n] = 0$ otherwise. Obviously, $\{p^0[n]\}_{n=1}^N$ is a feasible solution to problem (39), which guarantees a non-negative secrecy rate of the SR in each time slot and satisfies all the power-related constraints (39b)-(39d).

Up to now, we have obtained the initial point $\tilde{\mathcal{Z}}^0 \triangleq \{\boldsymbol{q}^0[n], p^0[n], \mu_s^0[n], \mu_e^0[n], t^0[n]\}_{n=1}^N$ for Algorithm 1.

IV. SIMULATION RESULTS

In this section, simulation results are provided to validate the performance of the UAV-to-SR secrecy communications

achieved by our proposed joint UAV trajectory optimization and transmit power control algorithm (denoted as J-T&P). For comparison, the following three benchmark schemes are selected.

- BET/P: best-effort trajectory design with power control. This scheme designs the UAV's trajectory in the heuristic best-effort manner described in Section III-D, and optimizes the transmit power by solving problem (39). Inspired by [20], the optimal solution to problem (39) can be expressed as

$$p^*[n] = \begin{cases} \min\left(\hat{p}[n], \tilde{p}[n], P_{\max}\right), & a_n \geq b_n, \\ 0, & a_n < b_n, \end{cases} \quad (40)$$

where

$$\hat{p}[n] = \left[\sqrt{\left(\frac{1}{2b_n} - \frac{1}{2a_n}\right)^2 + \frac{1}{\beta \ln 2}\left(\frac{1}{b_n} - \frac{1}{a_n}\right)} - \frac{1}{2b_n} - \frac{1}{2a_n}\right]^+, \quad (41)$$

$$\tilde{p}[n] = \min_{l \in \mathcal{L}} \frac{\Gamma_l}{\beta_0}\left(\|\boldsymbol{q}^0[n] - \boldsymbol{w}_{p,l}\|^2 + (H - H_l)^2\right)^{\alpha/2}. \quad (42)$$

In (41), $\beta \geq 0$ is a parameter ensuring $\frac{1}{N}\sum_{n=1}^{N} p^*[n] \leq \bar{P}$, which can be obtained by the bisection search.

- BET/NP: best-effort trajectory design without power control. For this scheme, the UAV's trajectory is designed in the foregoing best-effort manner, and the transmit power is set equally over time, i.e., $p[n] = p$, $\forall n$. Here, to satisfy the transmit power constraints and IT constraints, we set $p = \min\left(\bar{P}, \min_{n \in \mathcal{N}} \tilde{p}[n]\right)$.
- SLT/P: straight-line trajectory design with power control. In this scheme, the UAV flies from the initial to the final location along a straight line at a constant speed of $\left\|\boldsymbol{q}_F - \boldsymbol{q}_I\right\|/T$. Under this trajectory, the optimized transmit power is obtained by using (40).

Remark 3: We note that one scheme is also commonly considered as a baseline in the related works, which optimizes the UAV's trajectory with the transmit power fixed as $p[n] = \bar{P}, \forall n$. This scheme, however, is not applicable to our investigated problem due to the stringent IT constraints in (13f). Specifically, with given transmit power $p[n] = \bar{P}, \forall n$, (13f) can be rewritten as

$$\sqrt{\|\boldsymbol{q}[n] - \boldsymbol{w}_{p,l}\|^2 + (H - H_l)^2} \geq \left(\frac{\beta_0 \bar{P}}{\Gamma_l}\right)^{1/\alpha}, \forall n, l. \quad (43)$$

It is not difficult to see that when $\bar{P}$ is very large and/or Γ_l is very small, the UAV requires to fly far away from the PRs in each time slot to meet the IT constraints. However, in the case that the PRs locate near the UAV's initial/final location, pure trajectory optimization can not even generate a feasible solution to problem (P1). Therefore, this scheme is not considered in the performance comparison.

We consider a system with $K = 2$ Eves, whose estimated locations are marked by $'\triangle'$s as shown in Fig. 3, and

TABLE 1. Simulation parameters.

Description	Parameter and Value
UAV altitude	$H = 100$ m
UAV maximum speed	$V_{\max} = 10$ m/s
Duration of each time slot	$\delta = 0.5$ s
Channel gain	$\beta_0 = -30$ dB
Noise power	$\sigma^2 = -80$ dBm
Channel path-loss exponent	$\alpha = 2$
Maximum tolerance	$\epsilon = 10^{-4}$

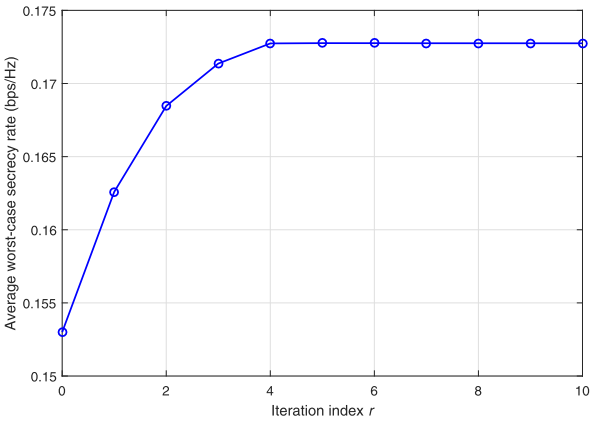

FIGURE 2. Convergence performance of the proposed J-T&P algorithm ($\bar{P} = 15$ dBm, $\Gamma = -80$ dBm and $T = 120$ s).

$\varepsilon_1 = 20$ m and $\varepsilon_2 = 80$ m. There are $L = 4$ PRs with equal height $H_l = 25$ m, $\forall l$, marked by $'\square'$s. The SR is located at $\boldsymbol{w}_s = [0, 0]^T$. The initial and final locations of the UAV are set as $\mathbf{q}_I = [-400, -200]^T$ and $\mathbf{q}_F = [400, -200]^T$, respectively. For illustration, the SR and the UAV's initial and final locations are marked by $'\circ'$, $'\times'$ and $'+'$, respectively. The peak transmit power limit is set as $P_{\max} = 4\bar{P}$. The IT thresholds are assumed to be identical for different PRs, i.e., $\Gamma_l = \Gamma, \forall l$. It is not difficult to verify that under this setup, the IT constraints are dominated by the PR nearest to the UAV at each time slot. The values of $\bar{P}$, Γ and T will be given in the following simulations. If not otherwise specified, other corresponding parameters in the simulations are summarized in Table 1.

We first numerically demonstrate the convergence performance of our proposed J-T&P algorithm in Fig. 2. Here, we set $\bar{P} = 15$ dBm, $\Gamma = -80$ dBm and $T = 120$ s. As we can see, the average worst-case secrecy rate obtained by the proposed J-T&P algorithm increases rapidly with the number of iterations and converges within around 6 iterations.

Fig. 3 shows the optimized UAV trajectories achieved by different algorithms, under different setups of $\bar{P}$ and Γ with the flight period set as $T = 120$ s. Notice that the UAV trajectories by the benchmark BET/P, BET/NP and SLT/P schemes do not change with different values of $\bar{P}$ and Γ. For the proposed J-T&P algorithm, when $\bar{P} = -5$ dBm and $\Gamma = -50$ dBm, it is observed that the UAV flies in an arc

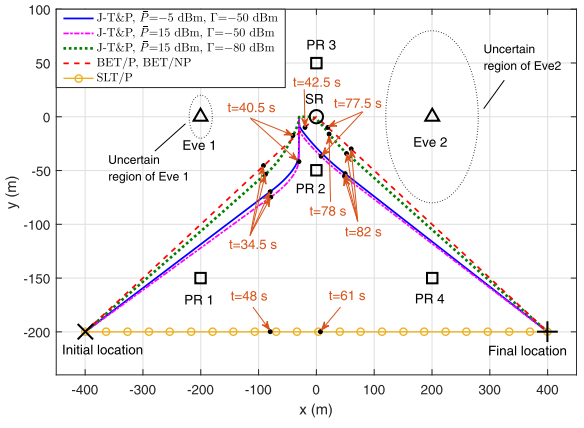

FIGURE 3. UAV's trajectories for T=120 s under different values of $\bar{P}$ and Γ.

path at speed $V_{\max}$ to keep away from Eve 1 and reach a certain point near the SR, then hovers there as long as it can, and finally flies at speed $V_{\max}$ to the final location along an arc path bypassing Eve 2. This observation is confirmed by the UAV's flight speed shown in Fig. 4(a). The optimized hovering point is on the left of the SR since the radius of the uncertain region of Eve 2 is larger than that of Eve 1. When the transmit power budget becomes larger (i.e., $\bar{P} = 15$ dBm and $\Gamma = -50$ dBm), it is interesting to note that the UAV moves further away from the Eves relative to the case with $\bar{P} = -5$ dBm. This observation indicates that moving further away from the Eves is conducive to maximizing the average secrecy rate when the UAV is allowed to transmit with a higher power. However, when $\bar{P} = 15$ dBm and Γ decreases to -80 dBm, the UAV chooses a trajectory that is further away from the PRs to reduce the co-channel interference power at them. This trajectory appears different from those in the previous two cases since the IT constraints become much more stringent.

Fig. 4 plots the corresponding UAV's transmit power and flight speeds of different algorithms versus time. In Fig. 4(b), it is observed that when $\bar{P}$ increases (i.e., $\bar{P} = 15$ dBm and $\Gamma = -50$ dBm), the proposed T-J&P and benchmark BET/P schemes reduce the transmit power to satisfy the IT constraints when the UAV approaches PR 2 (at time instants $t = 40.5$ s and $t = 77.5$ s for the proposed T-J&P algorithm, and at time instants $t = 42.5$ s and $t = 77.5$ s for the benchmark BET/P scheme). A similar observation can be made in Fig. 4(c) when $\bar{P} = 15$ dBm and Γ decreases to -80 dBm. We can also see from Fig. 4(c) that the transmit power by the proposed J-T&P algorithm is somewhat similar to that by the benchmark BET/P scheme, both of which are restricted to extremely low levels due to the stringent IT constraints. In addition, under different setups of $\bar{P}$ and Γ, we can see that when the UAV remains stationary at the hovering point, the proposed J-T&P algorithm sets the transmit power to a certain value to maximize the secrecy rate while satisfying the IT constraints at PRs 2 and 3. It is also worth mentioning that when the distance from the UAV to the nearest possible Eve is smaller than that to the SR, the J-T&P, BET/P and SLT/P schemes all set the transmit power to zero. This implies that the IT constraints at PRs 1 and 4 can always be met under any setup of the IT threshold Γ when $t \leq 34.5$ s and $t \geq 82$ s for the J-T&P and BET/P schemes, and when $t \leq 48$ s and $t \geq 61$ s for the SLT/P scheme. Finally, for the BET/NP scheme, we found that $p = \min\left(\bar{P}, \min_{n\in\mathcal{N}} \tilde{p}[n]\right) = \bar{P}$ when $\Gamma = -50$ dBm, and $p = \min\left(\bar{P}, \min_{n\in\mathcal{N}} \tilde{p}[n]\right) = \min_{n\in\mathcal{N}} \tilde{p}[n]$ when $\Gamma = -80$ dBm. This result indicates that the transmit power by the BET/NP scheme is dominantly limited by the maximum average transmit power constraint in the former case, but by the IT constraints in the latter case.

In Fig. 5, we plot the SR's average worst-case secrecy rates obtained by different algorithms versus the flight period T under different values of $\bar{P}$ and Γ. As expected, the proposed J-T&P algorithm always outperforms the other benchmark schemes, which shows the benefit of the joint trajectory optimization and power control in maximizing the SR's average secrecy rate. It is also observed that the secrecy rates of the J-T&P, BET/P and BET/NP schemes notably increase with T. This is because for these three schemes, the maximum secrecy rates are mainly achieved at their respective hovering points (see Fig. 3 and 4), and larger T enables the UAV to hover longer at such locations, thus resulting in higher average secrecy rates. Nevertheless, the average secrecy rate obtained by the SLT/P scheme remains unchanged regardless of T, since this scheme adopts a straight-line trajectory with a constant speed of $\left\|\boldsymbol{q}_F - \boldsymbol{q}_I\right\|/T$. The fairly large secrecy rate gap between the proposed J-T&P and benchmark SLT/P schemes demonstrates that the trajectory optimization is vital for improving the secrecy performance. Besides, we note that although the BET/P scheme in general outperforms the BET/NP scheme, the secrecy rate gap between them becomes very small when $\bar{P}$ increases from -5 to 15 dBm and $\Gamma = -50$ dBm. This observation suggests that the secrecy rate performance mainly relies on the UAV trajectory when $\bar{P}$ is high and $\Gamma = -50$ dBm.

Fig. 6 illustrates the SR's average worst-case secrecy rates achieved by different schemes versus the average transmit power $\bar{P}$ with $T = 120$ s. We first observe that the proposed J-T&P algorithm always obtains the highest secrecy rate, while the benchmark SLT/P scheme achieves the lowest one. It is also seen that when $\Gamma = -80$ dBm, the secrecy rates of all algorithms do not change with $\bar{P}$. The reason is that in this case, the stringent IT constraints dominate the transmit power, while the maximum average and peak transmit power constraints almost have no influence on it. When $\Gamma = -50$ dBm, the secrecy rates obtained by all algorithms increase with $\bar{P}$, as expected. This is due to the fact that when the IT constraints become less strict, a larger average transmit power budget offers a high flexibility in power allocating to achieve a higher secrecy rate. Furthermore, we note that the secrecy rates of all schemes tend to be saturated when $\bar{P}$ is high, and the BET/NP scheme yields almost the same performance as the BET/P scheme when $\bar{P} \geq 15$ dBm, which is consistent with the observation in Fig. 5(b). These results further demonstrate

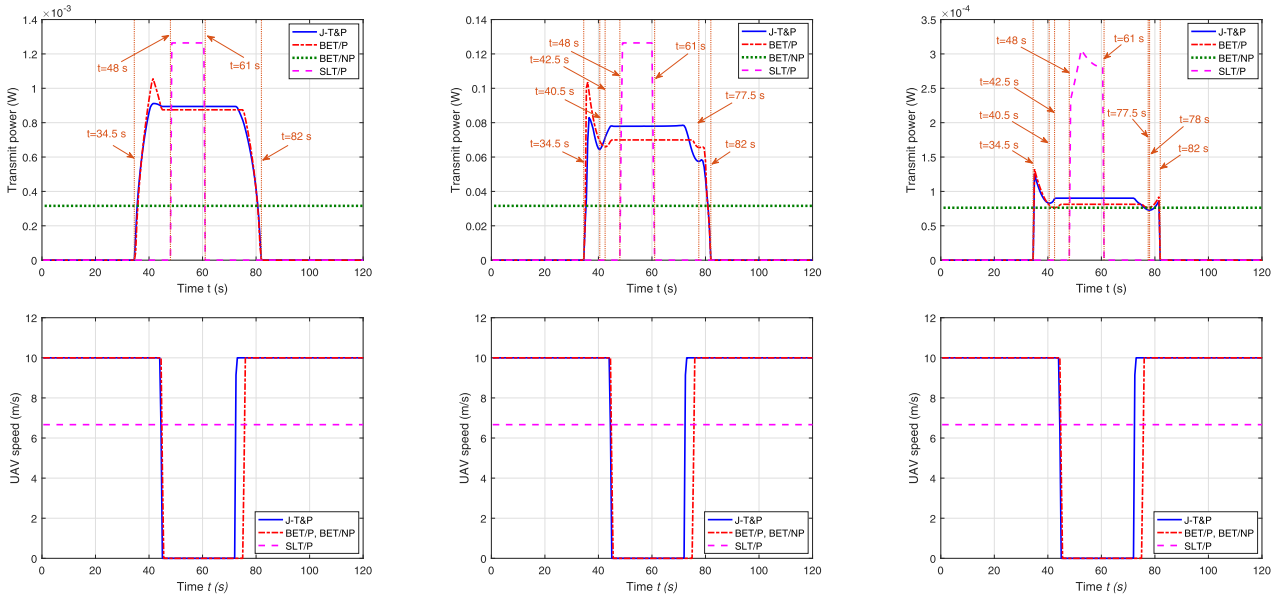

(a) $\bar{P} = -5$ dBm, $\Gamma = -50$ dBm (b) $\bar{P} = 15$ dBm, $\Gamma = -50$ dBm (c) $\bar{P} = 15$ dBm, $\Gamma = -80$ dBm

FIGURE 4. UAV's transmit power and flight speed versus time for $T = 120$ s under different values of $\bar{P}$ and Γ.

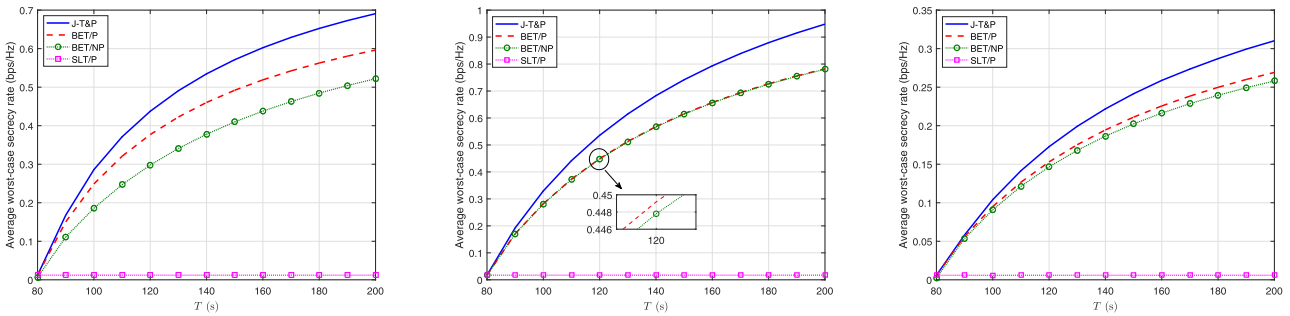

(a) $\bar{P} = -5$ dBm, $\Gamma = -50$ dBm (b) $\bar{P} = 15$ dBm, $\Gamma = -50$ dBm (c) $\bar{P} = 15$ dBm, $\Gamma = -80$ dBm

FIGURE 5. Average worst-case secrecy rate versus the flight period T under different values of $\bar{P}$ and Γ.

that in the high $\bar{P}$ regime when $\Gamma = -50$ dBm, the UAV trajectory plays a dominant role in the secrecy rate performance.

Fig. 7 shows the SR's average worst-case secrecy rates achieved by different schemes versus the IT threshold Γ with $T = 120$ s. As can be seen, under different values of $\bar{P}$, the secrecy rates of all schemes first increase with Γ when Γ is small and then remain constant when Γ exceeds a certain level. This result can be explained as follows. When Γ is small, the increase in Γ could weaken the IT constraints, which allows the UAV to transmit with a higher power, leading to an increase in the secrecy rate. When Γ is large enough, the transmit power is dominantly limited by the maximum average and peak transmit power constraints, thus further increasing Γ could not enlarge the feasible region of it any more. Besides, some similar observations as in Fig. 6 can be observed. Specifically, the secrecy rates of all algorithms do not change with $\bar{P}$ when Γ is sufficiently small, but increase with $\bar{P}$ when Γ becomes larger. The BET/NP scheme performs very close to the BET/P scheme over the whole Γ regime when $\bar{P} = 15$ dBm.

The effect of the number of PRs (L) on the SR's average worst-case secrecy rate achieved by the proposed J-T&P algorithm is shown in Fig. 8. In this simulation, each PR's horizontal location is randomly generated in a square region with a geometric center $(0, 0, 0)$ and each side being 200 m. It is assumed that all PRs have the same altitude 25 m. We set $\bar{P} = 10$ dBm, $\Gamma = -65$ dBm and $T = 120$ s. All other settings are the same as those in Fig. 3. All the results in Fig. 8 are obtained by averaging 100 random realizations. As expected, it is observed that the secrecy rate decreases as L increases. The reason for this result being that since the number of IT constraints increases with L, the feasible region of problem (P4) becomes smaller, resulting in a decrease in the secrecy rate.

Finally, we consider the effect of the Eves' location uncertainties on the secrecy rate performance. Fig. 9 plots the SR's

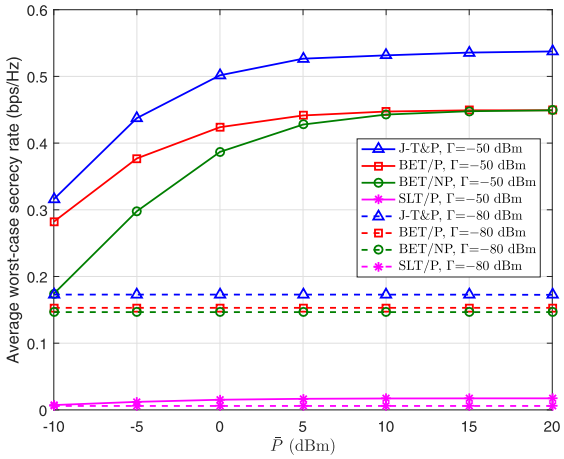

FIGURE 6. Average worst-case secrecy rate versus the average transmit power $\bar{P}$ for $T = 120$ s.

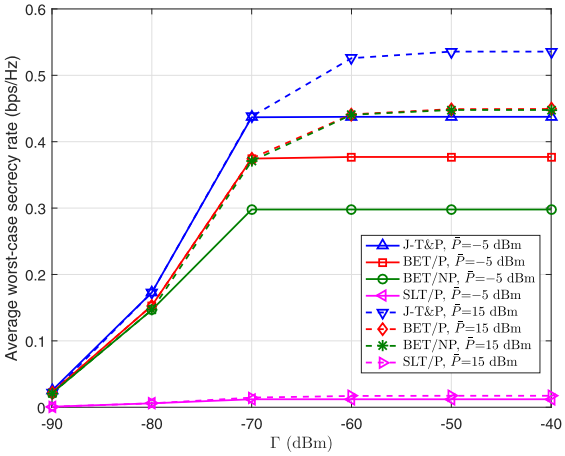

FIGURE 7. Average worst-case secrecy rate versus the IT threshold Γ for $T = 120$ s.

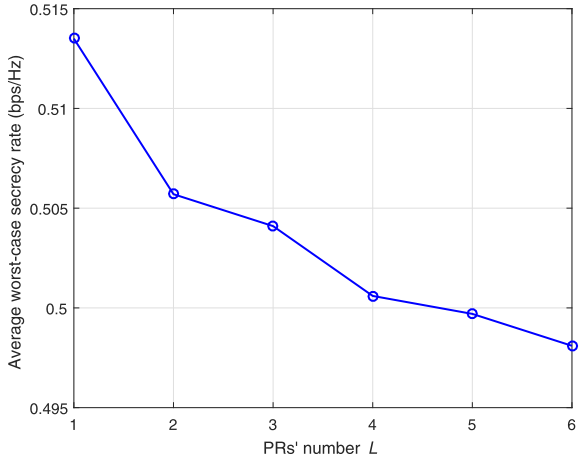

FIGURE 8. Average worst-case secrecy rate of the proposed J-T&P algorithm versus the number of PRs L ($\bar{P} = 10$ dBm, $\Gamma = -65$ dBm and $T = 120$ s).

average worst-case secrecy rates of the proposed J-T&P and benchmark BET/P schemes versus the radius of the uncertain region of Eve 1 ε_1 under different values of the radius of the

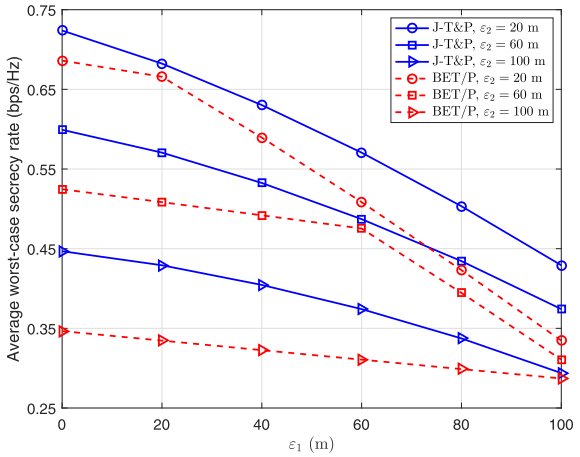

FIGURE 9. Average worst-case secrecy rates of the proposed J-T&P and benchmark BET/P schemes versus the radius of the uncertain region of Eve 1 ε_1 under different values of the radius of the uncertain region of Eve 2 ε_2 ($\bar{P} = 10$ dBm, $\Gamma = -65$ dBm and $T = 120$ s).

uncertain region of Eve 2 ε_2. In this simulation, we set $\bar{P} = 10$ dBm, $\Gamma = -65$ dBm and $T = 120$ s. All other settings are the same as those in Fig. 3. Intuitively, the secrecy rates of the two schemes decrease with the increasing of ε_1 or ε_2, which validates the motivation of the worst-case robust optimization. Besides, an interesting observation is that when $\varepsilon_1 = \varepsilon_2 = 20$, 60 and 100 m, the performance gap between the two schemes is small. The reasons are twofold. For one thing, since the distances from the estimated locations of Eves 1 and 2 to the SR are equal, $\varepsilon_1 = \varepsilon_2$ would make the optimized hovering point of the proposed J-T&P algorithm the same as that of the benchmark BET/P scheme (i.e., the position right above the SR). For another, the secrecy rates of both schemes are mainly achieved at their respective hovering points (see Fig. 3 and 4). Therefore, the same hovering point of the two schemes would result in their similar secrecy rates.

V. CONCLUSION

In this paper, we have studied the secrecy transmission in a UAV-aided CR network, where a secondary UAV transmitter sends confidential information to a ground SR in the presence of multiple co-channel primary terrestrial wireless communication links and multiple potential Eves with imperfect location information. We aim at maximizing the SR's average worst-case secrecy rate by jointly optimizing the UAV's transmit power and trajectory over a finite flight duration with given initial and final locations, subject to the mobility and transmit power constraints of the UAV, and the IT constraints at the PRs. To tackle the formulated non-convex semi-infinite optimization problem, we first prove that it can be simplified as a more tractable one with an explicit objective function. Then, an efficient iterative algorithm is proposed to obtain a locally optimal solution by leveraging the SCA technique. Simulation results show that the proposed joint design of the UAV trajectory and transmit power can achieve better secrecy rate performance as compared to other benchmark schemes without trajectory optimization and/or power control.

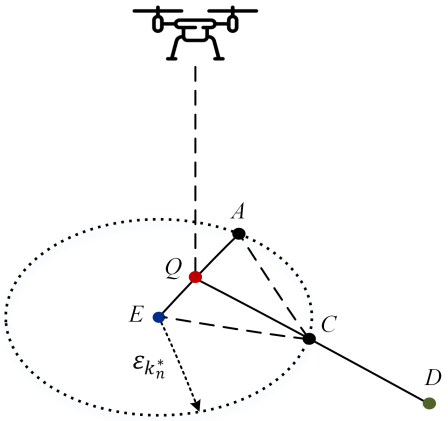

FIGURE 10. A geometric illustration of the considered scenario where the UAV is above the uncertain region of the k_n^*-th Eve. The exact location of the SR and the estimated location of the k_n^*-th Eve are denoted by points D and E, respectively. Denote the projection point of the UAV on the ground by Q. We set C as the interaction point of the uncertain region of the k_n^*-th Eve and the line segment that connects points Q and D. $|QA|$ and $|QD|$ correspond to $\left|\left\|q[n]-\tilde{w}_{e,k_n^*}\right\|-\varepsilon_{k_n^*}\right|$ and $\|q[n]-w_s\|$, respectively.

APPENDIXES

APPENDIX A
PROOF OF LEMMA 1

Let $\mathcal{K}_{n,M} \triangleq \left\{k \mid \|\boldsymbol{q}[n]-\tilde{\boldsymbol{w}}_{e,k}\| < \varepsilon_k\right\} \subseteq \mathcal{K}$ with cardinality $M \geq 1$ be the subset of the Eves.[6] We mark the strongest Eve that gains $\min_{k\in\mathcal{K}_{n,M}} \left|\|\boldsymbol{q}[n]-\tilde{\boldsymbol{w}}_{e,k}\|-\varepsilon_k\right|$ as the k_n^*-th one. To facilitate the analysis, we give a geometric illustration of the considered scenario where the UAV is above the uncertain region of the k_n^*-th Eve (i.e., $\|\boldsymbol{q}[n]-\tilde{\boldsymbol{w}}_{e,k_n^*}\| < \varepsilon_{k_n^*}$) in Fig. 10.[7] According to the geometric properties shown in Fig. 10, it follows that

$$|EQ|+|QA| = |EA| = |EC| < |EQ|+|QC|. \tag{44}$$

Then we can derive from (44) that $|QA| < |QC|$. Since $|QC| < |QD|$, we have $|QA| < |QD|$, i.e.,

$$\left|\left\|\boldsymbol{q}[n]-\tilde{\boldsymbol{w}}_{e,k_n^*}\right\|-\varepsilon_{k_n^*}\right| < \|\boldsymbol{q}[n]-\boldsymbol{w}_s\|. \tag{45}$$

Furthermore, it is clear that $\min_{k\in\mathcal{K}} \left|\|\boldsymbol{q}[n]-\tilde{\boldsymbol{w}}_{e,k}\|-\varepsilon_k\right| \leq \left|\left\|\boldsymbol{q}[n]-\tilde{\boldsymbol{w}}_{e,k_n^*}\right\|-\varepsilon_{k_n^*}\right|$ since $k_n^* \in \mathcal{K}_{n,M} \subseteq \mathcal{K}$. Accordingly, we have

$$\min_{k\in\mathcal{K}} \left|\|\boldsymbol{q}[n]-\tilde{\boldsymbol{w}}_{e,k}\|-\varepsilon_k\right| < \|\boldsymbol{q}[n]-\boldsymbol{w}_s\|. \tag{46}$$

This lemma is thus proved.

APPENDIX B

Problem (P3) is equivalent to (P2) since at the optimal solution $\mathcal{Z}^* \triangleq \{\boldsymbol{q}^*[n], p^*[n], \mu_s^*[n], \mu_e^*[n]\}_{n=1}^N$ to (P3), we must have the following equalities:

$$\mu_s^*[n] = (\|\boldsymbol{q}^*[n]-\boldsymbol{w}_s\|^2+H^2)^{\alpha/2}, \forall n, \tag{47}$$

[6]Since the sets of the possible locations of the Eves may have a non-empty intersection, the UAV may be above the uncertain regions of more than one Eve in time slot n.

[7]To ensure a non-trivial secrecy rate, we assume that the SR is not in the uncertain region of any Eve.

$$\mu_e^*[n] = (\min_{k\in\mathcal{K}} |\,\|\boldsymbol{q}^*[n]-\tilde{\boldsymbol{w}}_{e,k}\|-\varepsilon_k|^2+H^2)^{\alpha/2}, \forall n. \tag{48}$$

These can be proved by contradiction. Specifically, if there exists a $\mu_s^*[n]$ such that $\mu_s^*[n] > (\|\boldsymbol{q}^*[n]-\boldsymbol{w}_s\|^2+H^2)^{\alpha/2}$ and/or a $\mu_e^*[n]$ such that $\mu_e^*[n] < (\min_{k\in\mathcal{K}}|\,\|\boldsymbol{q}^*[n]-\tilde{\boldsymbol{w}}_{e,k}\|-\varepsilon_k|^2+H^2)^{\alpha/2}$, we can further improve the objective value of problem (P3) by decreasing $\mu_s^*[n]$ to $(\|\boldsymbol{q}^*[n]-\boldsymbol{w}_s\|^2+H^2)^{\alpha/2}$ and/or increasing $\mu_e^*[n]$ to $(\min_{k\in\mathcal{K}}|\,\|\boldsymbol{q}^*[n]-\tilde{\boldsymbol{w}}_{e,k}\|-\varepsilon_k|^2+H^2)^{\alpha/2}$, which leads to a contradiction that $\mu_s^*[n]$ and/or $\mu_e^*[n]$ are the optimal solutions. This thus proves that the equalities in (47) and (48) hold. Therefore, problem (P3) and (P2) are equivalent.

APPENDIX C

Consider a function $g(\mathbf{x}) = \|\mathbf{x}-\mathbf{b}\|^2+c$, where $\mathbf{x} \in \mathbb{R}^n$, $\mathbf{b} \in \mathbb{R}^n$ and $c \geq 0$. It is well known that $g(\mathbf{x})$ is a convex function with respect to $\mathbf{x}$. Since $g(\mathbf{x})$ is convex and non-negative, the convexity of $g(\mathbf{x})^{\alpha/2}$ is guaranteed with $\frac{\alpha}{2} \geq 1$ according to the composition results given in Example 3.13 in [43, Sec. 3.2.4]. As a result, $\left(\|\boldsymbol{q}[n]-\boldsymbol{w}_s\|^2+H^2\right)^{\alpha/2}$ and $\left(\|\boldsymbol{q}[n]-\boldsymbol{w}_{p,l}\|^2+(H-H_l)^2\right)^{\alpha/2}$ are all convex functions with respect to $\boldsymbol{q}[n]$.

APPENDIX D

Problem (P4) is equivalent to (P3) since at the optimal solution $\tilde{\mathcal{Z}}^* \triangleq \{\boldsymbol{q}^*[n], p^*[n], \mu_s^*[n], \mu_e^*[n], t^*[n]\}_{n=1}^N$ to (P4), we must have the following equalities:

$$\mu_e^*[n] = t^*[n]^{\alpha/2}, \quad \forall n, \tag{49}$$

$$t^*[n] = \min_{k\in\mathcal{K}} |\,\|\boldsymbol{q}^*[n]-\tilde{\boldsymbol{w}}_{e,k}\|-\varepsilon_k|^2+H^2, \quad \forall n. \tag{50}$$

These can be proved by contradiction. Specifically, if there exists a $\mu_e^*[n]$ such that $\mu_e^*[n] < t^*[n]^{\alpha/2}$, we can further improve the objective value of (P4) by increasing $\mu_e^*[n]$ to $t^*[n]^{\alpha/2}$, resulting in a contradiction that $\mu_e^*[n]$ is the optimal solution. This proves that the equalities in (49) hold. Besides, if there exists a $t^*[n]$ such that $t^*[n] < \min_{k\in\mathcal{K}}|\,\|\boldsymbol{q}^*[n]-\tilde{\boldsymbol{w}}_{e,k}\|-\varepsilon_k|^2+H^2$, we can always find another $\hat{t}[n]$ such that $\hat{t}[n] = \min_{k\in\mathcal{K}}|\,\|\boldsymbol{q}^*[n]-\tilde{\boldsymbol{w}}_{e,k}\|-\varepsilon_k|^2+H^2$. By this newly chosen $\hat{t}[n]$ and the proved equalities in (49), we can find another $\hat{\mu}_e[n]$ such that $\hat{\mu}_e[n] = \hat{t}[n]^{\alpha/2} > t^*[n]^{\alpha/2} = \mu_e^*[n]$. Obviously, we can obtain a strictly larger objective value of (P4) with the newly chosen $\hat{\mu}_e[n]$, which is in contradiction to the assumption that $\mu_e^*[n]$ and $t^*[n]$ are the optimal solutions. This proves that the equalities in (50) hold. Therefore, problem (P4) and (P3) are equivalent.

REFERENCES

[1] Y. Zeng, R. Zhang, and T. J. Lim, "Wireless communications with unmanned aerial vehicles: Opportunities and challenges," *IEEE Commun. Mag.*, vol. 54, no. 5, pp. 36–42, May 2016.

[2] Q. Wu and R. Zhang, "Common throughput maximization in UAV-enabled OFDMA systems with delay consideration," *IEEE Trans. Commun.*, vol. 66, no. 12, pp. 6614–6627, Dec. 2018.

[3] Y. Zeng, R. Zhang, and T. J. Lim, "Throughput maximization for UAV-enabled mobile relaying systems," *IEEE Trans. Commun.*, vol. 64, no. 12, pp. 4983–4996, Dec. 2016.

[4] C. Zhan, Y. Zeng, and R. Zhang, "Energy-efficient data collection in UAV enabled wireless sensor network," *IEEE Wireless Commun. Lett.*, vol. 7, no. 3, pp. 328–331, Jun. 2018.

[5] A. Al-Hourani, S. Kandeepan, and S. Lardner, "Optimal LAP altitude for maximum coverage," *IEEE Wireless Commun. Lett.*, vol. 3, no. 6, pp. 569–572, Dec. 2014.

[6] M. Mozaffari, W. Saad, M. Bennis, and M. Debbah, "Efficient deployment of multiple unmanned aerial vehicles for optimal wireless coverage," *IEEE Commun. Lett.*, vol. 20, no. 8, pp. 1647–1650, Aug. 2016.

[7] J. Lyu, Y. Zeng, R. Zhang, and T. J. Lim, "Placement optimization of UAV-mounted mobile base stations," *IEEE Commun. Lett.*, vol. 21, no. 3, pp. 604–607, Mar. 2017.

[8] M. Alzenad, A. El-Keyi, F. Lagum, and H. Yanikomeroglu, "3-D placement of an unmanned aerial vehicle base station (UAV-BS) for energy-efficient maximal coverage," *IEEE Wireless Commun. Lett.*, vol. 6, no. 4, pp. 434–437, Aug. 2017.

[9] M. Alzenad, A. El-Keyi, and H. Yanikomeroglu, "3-D placement of an unmanned aerial vehicle base station for maximum coverage of users with different QoS requirements," *IEEE Wireless Commun. Lett.*, vol. 7, no. 1, pp. 38–41, Feb. 2018.

[10] J. Sun and C. Masouros, "Deployment strategies of multiple aerial BSs for user coverage and power efficiency maximization," *IEEE Trans. Commun.*, vol. 67, no. 4, pp. 2981–2994, Apr. 2019.

[11] Y. Zeng, X. Xu, and R. Zhang, "Trajectory design for completion time minimization in UAV-enabled multicasting," *IEEE Trans. Wireless Commun.*, vol. 17, no. 4, pp. 2233–2246, Apr. 2018.

[12] Y. Sun, D. Xu, D. W. K. Ng, L. Dai, and R. Schober, "Optimal 3D-trajectory design and resource allocation for solar-powered UAV communication systems," *IEEE Trans. Commun.*, vol. 67, no. 6, pp. 4281–4298, Jun. 2019.

[13] Y. Zeng, J. Xu, and R. Zhang, "Energy minimization for wireless communication with rotary-wing UAV," *IEEE Trans. Wireless Commun.*, vol. 18, no. 4, pp. 2329–2345, Apr. 2019.

[14] Q. Wu, Y. Zeng, and R. Zhang, "Joint trajectory and communication design for multi-UAV enabled wireless networks," *IEEE Trans. Wireless Commun.*, vol. 17, no. 3, pp. 2109–2121, Mar. 2018.

[15] J. Xu, Y. Zeng, and R. Zhang, "UAV-enabled wireless power transfer: Trajectory design and energy optimization," *IEEE Trans. Wireless Commun.*, vol. 17, no. 8, pp. 5092–5106, Aug. 2018.

[16] F. Zhou, Y. Wu, R. Q. Hu, and Y. Qian, "Computation rate maximization in UAV-enabled wireless-powered mobile-edge computing systems," *IEEE J. Sel. Areas Commun.*, vol. 36, no. 9, pp. 1927–1941, Sep. 2018.

[17] S. Jeong, O. Simeone, and J. Kang, "Mobile edge computing via a UAV-mounted cloudlet: Optimization of bit allocation and path planning," *IEEE Trans. Veh. Technol.*, vol. 67, no. 3, pp. 2049–2063, Mar. 2018.

[18] C. You and R. Zhang, "3D trajectory optimization in Rician fading for UAV-enabled data harvesting," *IEEE Trans. Wireless Commun.*, vol. 18, no. 6, pp. 3192–3207, Jun. 2019.

[19] Q. Wu, W. Mei, and R. Zhang, "Safeguarding wireless network with UAVs: A physical layer security perspective," *IEEE Wireless Commun.*, vol. 26, no. 5, pp. 12–18, Oct. 2019.

[20] P. K. Gopala, L. Lai, and H. El Gamal, "On the secrecy capacity of fading channels," in *Proc. IEEE Int. Symp. Inf. Theory*, Jun. 2007, pp. 4687–4698.

[21] X. Sun, D. W. K. Ng, Z. Ding, Y. Xu, and Z. Zhong, "Physical layer security in UAV systems: Challenges and opportunities," *IEEE Wireless Commun.*, vol. 26, no. 5, pp. 40–47, Oct. 2019.

[22] G. Zhang, Q. Wu, M. Cui, and R. Zhang, "Securing UAV communications via joint trajectory and power control," *IEEE Trans. Wireless Commun.*, vol. 18, no. 2, pp. 1376–1389, Feb. 2019.

[23] Z. Li, M. Chen, C. Pan, N. Huang, Z. Yang, and A. Nallanathan, "Joint trajectory and communication design for secure UAV networks," *IEEE Commun. Lett.*, vol. 23, no. 4, pp. 636–639, Apr. 2019.

[24] Q. Wang, Z. Chen, H. Li, and S. Li, "Joint power and trajectory design for physical-layer secrecy in the UAV-aided mobile relaying system," *IEEE Access*, vol. 6, pp. 62849–62855, Oct. 2018.

[25] F. Cheng, G. Gui, N. Zhao, Y. Chen, J. Tang, and H. Sari, "UAV-relaying-assisted secure transmission with caching," *IEEE Trans. Commun.*, vol. 67, no. 5, pp. 3140–3153, May 2019.

[26] L. Xiao, Y. Xu, D. Yang, and Y. Zeng, "Secrecy energy efficiency maximization for UAV-enabled mobile relaying," *IEEE Trans. Green Commun. Netw.*, to be published, doi: 10.1109/TGCN.2019.2949802.

[27] Y. Gao, H. Tang, B. Li, and X. Yuan, "Joint trajectory and power design for UAV-enabled secure communications with no-fly zone constraints," *IEEE Access*, vol. 7, pp. 44459–44470, Apr. 2019.

[28] A. Li, Q. Wu, and R. Zhang, "UAV-enabled cooperative jamming for improving secrecy of ground wiretap channel," *IEEE Wireless Commun. Lett.*, vol. 8, no. 1, pp. 181–184, Feb. 2019.

[29] H. Lee, S. Eom, J. Park, and I. Lee, "UAV-aided secure communications with cooperative jamming," *IEEE Trans. Veh. Technol.*, vol. 67, no. 10, pp. 9385–9392, Oct. 2018.

[30] Y. Cai, F. Cui, Q. Shi, M. Zhao, and G. Y. Li, "Dual-UAV-Enabled secure communications: Joint trajectory design and user scheduling," *IEEE J. Sel. Areas Commun.*, vol. 36, no. 9, pp. 1972–1985, Sep. 2018.

[31] X. Zhou, Q. Wu, S. Yan, F. Shu, and J. Li, "UAV-enabled secure communications: Joint trajectory and transmit power optimization," *IEEE Trans. Veh. Technol.*, vol. 68, no. 4, pp. 4069–4073, Apr. 2019.

[32] M. Hua, Y. Wang, Q. Wu, H. Dai, Y. Huang, and L. Yang, "Energy-efficient cooperative secure transmission in multi-UAV-enabled wireless networks," *IEEE Trans. Veh. Technol.*, vol. 68, no. 8, pp. 7761–7775, Aug. 2019.

[33] M. Cui, G. Zhang, Q. Wu, and D. W. K. Ng, "Robust trajectory and transmit power design for secure UAV communications," *IEEE Trans. Veh. Technol.*, vol. 67, no. 9, pp. 9042–9046, Sep. 2018.

[34] C. Zhong, J. Yao, and J. Xu, "Secure UAV communication with cooperative jamming and trajectory control," *IEEE Commun. Lett.*, vol. 23, no. 2, pp. 286–289, Feb. 2019.

[35] Y. Zhou, P. L. Yeoh, H. Chen, Y. Li, R. Schober, L. Zhuo, and B. Vucetic, "Improving physical layer security via a UAV friendly jammer for unknown eavesdropper location," *IEEE Trans. Veh. Technol.*, vol. 67, no. 11, pp. 11280–11284, Nov. 2018.

[36] Y. Cai, Z. Wei, R. Li, D. W. Kwan Ng, and J. Yuan, "Energy-efficient resource allocation for secure UAV communication systems," in *Proc. IEEE Wireless Commun. Netw. Conf. (WCNC)*, Apr. 2019, pp. 1–8.

[37] T. Bai, J. Wang, Y. Ren, and L. Hanzo, "Energy-efficient computation offloading for secure UAV-Edge-Computing systems," *IEEE Trans. Veh. Technol.*, vol. 68, no. 6, pp. 6074–6087, Jun. 2019.

[38] A. Goldsmith, S. A. Jafar, I. Maric, and S. Srinivasa, "Breaking spectrum gridlock with cognitive radios: An information theoretic perspective," *Proc. IEEE*, vol. 97, no. 5, pp. 894–914, May 2009.

[39] Y. Huang, W. Mei, J. Xu, L. Qiu, and R. Zhang, "Cognitive UAV communication via joint maneuver and power control," *IEEE Trans. Commun.*, vol. 67, no. 11, pp. 7872–7888, Nov. 2019.

[40] D. Chi-Nguyen, P. N. Pathirana, M. Ding, and A. Seneviratne, "Secrecy performance of the UAV enabled cognitive relay network," in *Proc. IEEE 3rd Int. Conf. Commun. Inf. Syst. (ICCIS)*, Dec. 2018, pp. 117–121.

[41] P. X. Nguyen, H. V. Nguyen, V.-D. Nguyen, and O.-S. Shin, "UAV-enabled jamming noise for achieving secure communications in cognitive radio networks," in *Proc. 16th IEEE Annu. Consum. Commun. Netw. Conf. (CCNC)*, Jan. 2019, pp. 1–6.

[42] R. Zhang, Y.-C. Liang, and S. Cui, "Dynamic resource allocation in cognitive radio networks," *IEEE Signal Process. Mag.*, vol. 27, no. 3, pp. 102–114, May 2010.

[43] S. Boyd and L. Vandenberghe, *Convex Optimization*. Cambridge, U.K.: Cambridge Univ. Press, 2004.

[44] Y. Zeng and R. Zhang, "Energy-efficient UAV communication with trajectory optimization," *IEEE Trans. Wireless Commun.*, vol. 16, no. 6, pp. 3747–3760, Jun. 2017.

[45] B. V. Der Bergh, A. Chiumento, and S. Pollin, "LTE in the sky: Trading off propagation benefits with interference costs for aerial nodes," *IEEE Commun. Mag.*, vol. 54, no. 5, pp. 44–50, May 2016.

[46] R. Sun, D. W. Matolak, and W. Rayess, "Air-ground channel characterization for unmanned aircraft systems—Part IV: Airframe shadowing," *IEEE Trans. Veh. Technol.*, vol. 66, no. 9, pp. 7643–7652, Sep. 2017.

[47] X. Lin, V. Yajnanarayana, S. D. Muruganathan, S. Gao, H. Asplund, H.-L. Maattanen, M. Bergstrom, S. Euler, and Y.-P.-E. Wang, "The sky is not the limit: LTE for unmanned aerial vehicles," *IEEE Commun. Mag.*, vol. 56, no. 4, pp. 204–210, Apr. 2018.

[48] 3GPP. *Enhanced LTE Support for Aerial Vehicles*. Accessed: Jul. 16, 2017. [Online]. Available: ftp://www.3gpp.org/specs/archive/36_series/36.777

[49] U. Mengali and A. N. D'Andrea, *Synchronization Techniques for Digital Receivers*. New York, NY, USA: Springer, 1997.

[50] K.-Y. Wang, A. M.-C. So, T.-H. Chang, W.-K. Ma, and C.-Y. Chi, "Outage constrained robust transmit optimization for multiuser MISO downlinks: Tractable approximations by conic optimization," *IEEE Trans. Signal Process.*, vol. 62, no. 21, pp. 5690–5705, Nov. 2014.

YING GAO received the B.Eng. degree from the Nanjing University of Science and Technology (NUST), China, in 2016. She is currently pursuing the Ph.D. degree with the Shanghai Institute of Microsystem and Information Technology, Chinese Academy of Sciences in the University of Chinese Academy of Sciences. Her current research interest includes unmanned aerial vehicle (UAV) communications.

HONGYING TANG received the Ph.D. degree from Shanghai Jiao Tong University (SJTU), China, in 2015. She is currently an Engineer with the Science and Technology on Microsystem Laboratory, Shanghai Institute of Microsystem and Information Technology, Chinese Academy of Sciences. Her research interest includes unmanned aerial vehicle (UAV) communications.

BAOQING LI received the Ph.D. degree from the State Key Laboratory of Transducer Technology, Shanghai Institute of Metallurgy, Chinese Academy of Sciences, Shanghai, China, in 2000. He is currently a Professor and a Ph.D. Supervisor with the Shanghai Institute of Microsystem and Information Technology, Chinese Academy of Sciences. His research interest includes the application of wireless sensor networks.

XIAOBING YUAN received the Ph.D. degree from the Changchun Institute of Optics, Fine Mechanics, and Physics, Chinese Academy of Sciences, Changchun, China, in 2000. He is currently a Professor and a Ph.D. Supervisor with the Shanghai Institute of Microsystem and Information Technology, Chinese Academy of Sciences. His research interests include wireless sensor networks and information transmission processing.